International Doctorate in Atomic and Molecular Photonics
Cycle XXXII

Coordinator Prof. Francesco S. Cataliotti

Experiments on random lasers: a novel method for super-resolution spectroscopy

(FIS/03)

Candidate
Dott. Alice Boschetti

Supervisor
Prof. Diederik S. Wiersma

Coordinator
Prof. Francesco S. Cataliotti

2016-2019

Experiments on random lasers: a novel method for super-resolution spectroscopy
International Doctorate in Atomic and Molecular Photonics, November 2019
Coordinator: Prof. Francesco S. Cataliotti
Supervisor: Prof. Diederik S. Wiersma

Università degli Studi di Firenze
Laboratorio Europeo di Spettroscopia non Lineare
Via Nello Carrara 1, Sesto Fiorentino, Firenze

Reviewers: Prof. Allard Mosk and Prof. Ori Katz

This three-year Phd course led to the following works:

A. Boschetti, A. Taschin, P. Bartolini, A.K. Tiwari, L. Pattelli, R. Torre, D.S. Wiersma. Spectral super-resolution spectroscopy using a random laser. *Nat. Photon.,* in press (2019).

A. Boschetti, A. Taschin, P. Bartolini, L. Pattelli, R. Torre, D.S. Wiersma. Metodo ed apparato per la misurazione della risposta spettrale di un campione basato su un random laser come sorgente di illuminazione. Patent priority number 10201900014748 (2019).

A. Boschetti, A. Taschin, P. Bartolini, L. Pattelli, R. Torre, D.S. Wiersma. Transient cavity formation in random lasing suspensions (In preparation, 2019).

Contents

1 Introduction **1**

2 The physics of random lasers **3**
2.1 Light scattering by particles 3
2.2 Scattering and gain in random lasers 5
2.2.1 Emission properties of random lasers 9
2.2.2 Random laser with dye solutions 12
2.3 Optimization and application of random lasers 17

3 Fabry-Pérot-like resonances in weakly scattering medium with gain **25**
3.1 Introduction 25
3.2 Experimental results 27
3.3 Discussion 38

4 Optical super-resolution **43**
4.1 Super-resolution techniques for imaging and spectroscopy 43
4.2 A new concept of spectral super-resolution 47
4.2.1 Simulation of a spectral-super resolution experiment 48
4.2.2 Statistics and noise levels for spectral reconstruction 51
4.3 Appendix 55

5 Experimental demonstration of super-resolved spectral reconstruction using a random laser **63**
5.1 Description of the random laser sample 63
5.2 Experimental set-up 67
5.3 Analysis 69
5.3.1 Validity limits and fundamental bounds 74

5.3.2 The roles of sparsity and randomness 75
5.4 Comparison with state of the art techniques 75
Appendices 79
A Random laser threshold and stable distributions 79
B MATLAB code for peak selection 81

Chapter 1

Introduction

Ever since the invention of fire, the human race has engaged into a quest for increasingly more powerful, efficient and versatile light sources, going well beyond the visibile frequency range. 2020 will mark the 60^{th} anniversary of the first laser, but this invention would not have been possible without our understanding of light as a form of electromagnetic radiation. From that moment lasers have became progressively smaller, tunable, more robust and energy efficient as well as less expensive. The technology has expanded the wavelength range well beyond visible and infrared light and in the choice of materials used. This work deals with random lasers, a peculiar class of coherent light sources with very little apparent resemblance to conventional lasers. Differently from conventional lasers, random lasers lack an external cavity and the comprehension of their lasing mechanisms has challenged the scientific community for several years. Despite their unique properties [1–4], it is unlikely that random lasers will achieve the success of conventional lasers unless the physics regulating their working mechanism is fully explained and chaotic emission properties are eventually controlled. Far from addressing the many open questions in the field of random lasing, in this work we report on a few experimental insights about random laser emission and propose a novel spectroscopy technique that employs random lasers as the ideal source of illumination. In particular, we will describe the application of a random laser working in the pulsed chaotic regime to achieve spectrally super-resolved reconstruction of an arbitrary transfer function. The key functional properties enabling our application such as the uncorrelated lasing mode frequencies, their sub-nanometer width and their sparse distribution

above the active medium curve, together with other typical emission characteristics of a random laser are described in Chapter 2. An overview about the more recent applications of random lasers and attempts to engineer their emission characteristics is addressed in the last section. Chapter 3 extends the discussion of the emission properties by reporting on the experimental observation in dye-solution-based random lasers of occasional periodic, resonator-like emission spectra among the chaotic ones. We elucidate the possible mechanism underlying this phenomenon, also taking into account previous attempts reported in the literature to explain its origin. Chapter 4 describes our practical application of the random laser and discusses its validation from a numerical perspective. The chapter comprises an introduction to the most widespread super-resolution techniques and presents the new idea of spectral super-resolution using the emissions of the random laser. The last sections of this chapter are dedicated to numerical calculations evaluating the robustness against experimental noise and the limits of applicability of the method. The spectral super-resolved numerical reconstruction of a simple transmission function is demonstrated at resolution exceeding that imposed by the instrumental response function. We discuss in detail the goodness of the reconstruction as a function of the instrumental response shapes, the number of random laser spectra required, as well as the statistic of the intensities of the laser peaks. Finally Chapter 5 shows the experimental results obtained in the lab providing the first proof-of-concept of the super-resolved spectral reconstruction of a simple transmission function, with a roughly threefold resolution enhancement with respect to the spectrometer spectral response.

Chapter 2

The physics of random lasers

2.1 Light scattering by particles

When light waves interact with matter they can undergo scattering and absorption depending on the properties of the material. In the elastic scattering process light changes its propagation direction without changing its frequency. Reflection can be described as a scattering event where the incidence and output angles are the same. A blade of grass looks green because it scatters light efficiently at that frequency, while blue and red light is absorbed for photosynthesis, meaning that its energy is converted into a different form and is no longer present as electromagnetic wave.

Light propagating through a homogeneous medium is not scattered, only inhomogeneities cause scattering. Any real medium is inhomogeneous, since it contains discrete electric charges that are set into oscillation when illuminated by an electromagnetic wave. The accelerated charges radiate electromagnetic waves in all directions, this radiation is known as scattered radiation.

In a single scattering event an oscillating field is applied to a single particle that induces dipole moments in its sub-regions. These dipoles oscillate at the frequency of the applied field and emit secondary radiation in all directions. Along a certain direction, the total scattered field is obtained by superposing the scattered wavelets, which maintain definite phase differences, meaning that scattering by dipoles is coherent. The phase relations change for different scattering directions and the scattered field varies with scattering direction.

Multiple scattering phenomena occur when light, after penetrating an optical material, is scattered many times before exiting again. Multiple scattering is a well-known phenomenon that determines the appearance of opaque materials such as clouds, white paint, milk and powders. When light is scattered multiple times inside a disordered material its propagation can be described with a random walk [5]. In this framework, two main length scales describing scattering are the scattering mean free path l_s defined as the average distance that light travels between two consecutive scattering events, and the transport mean free path l_t, the average distance a wave travels before its direction of propagation is randomized. These two length scales are related by the relation:

$$l_t = \frac{l_s}{1 - \langle \cos\theta \rangle} \tag{2.1}$$

$\langle \cos\theta \rangle$ is the average cosine of the scattering angle, which can be found from the differential scattering cross section. For Rayleigh scattering $\langle \cos\theta \rangle = 0$ and $l_t = l_s$, while in the Mie scattering regime $\langle \cos\theta \rangle$ can span a larger range of values (even negative), with typical values around $\langle \cos\theta \rangle \approx 0.5$, and $l_t \approx 2l_s$ [6].

Multiple scattered waves undergoing a random walk maintain their coherence. This means that even if a material is strongly disordered, interference effects occur in a deterministic fashion. A classic example of interference in presence of multiple scattered light is that of a laser speckle from a disordered medium.

When the length scales of the medium are long compared to l_t, it is convenient to consider multiple scattering as diffusion of light, with the diffusion coefficient given by $D = \frac{cl_t}{3}$ with c the effective speed of light in the dielectric medium. However the diffusion model takes into account probability rather than amplitude, and interference of waves can not always be neglected. In the case of optical waves propagating through a disordered dielectric medium, this interference effect has been accurately demonstrated by a series of experiments initiated by Kuga & Ishimaru [7], Albada & Lagendijk [8] and Wolf & Maret [9], who reported on the observation of coherent backscattering. They measured the angular dependence of the backscattered intensity of laser light entering in a disordered dielectric sample.

When wave interference plays an important role in determining transport, as it does in coherent backscattering, the transport of wave energy is not diffusive in the simple sense of a photon performing the classical random walk. When ap-

plying the concepts of classical diffusion to even more complicated situations, we must consider the coherence properties of the illuminated sample. Typically, it is reasonable to expect that scatterers that are very distant do not on average cause large interference corrections to the classical diffusion picture. Instead, changes in distant scatterers can give rise to significant fluctuations about the average. Thus there exists a coherence length l_{coh} that represents the scale on which we must incorporate interference effects in order to determine the effective diffusion coefficient within the coherence volume. By changing the scale of the sample L, the number of possible interfering paths changes, then the effective diffusion coefficient $D(L)$ depends also on the macroscopic scale. When L is long compared to l_{coh}, the photon is considered in diffusive motion, with a small renormalization value for the diffusion coefficient, $D(L) \sim \frac{cl_{\mathrm{t}}}{3}(l_{\mathrm{t}}/l_{\mathrm{coh}})$ [10]. The most striking consequence of the dependence of D on L is that, for 1D and 2D systems, $\lim_{L\to\infty} D(L) = 0$. This means that, at least for low dimensional systems where $l_{\mathrm{t}} \ll L \ll l_{\mathrm{coh}}$, the diffusive process may come to a halt because of interference effects and light localization effects emerge [5].

2.2 Scattering and gain in random lasers

A conventional laser is based on an active medium that provides optical gain through stimulated emission and an optical cavity that partially traps the light and induces a coherent feedback. When the optical gain in the cavity becomes larger than the losses, the system reaches the threshold and lases. For what concerns light scattering inside a gain medium, from the point of view of conventional laser action it has always been considered undesirable because scattering removes photons from the lasing mode of a laser cavity. However, in a strongly scattering gain medium, light scattering plays a positive role since multiple scattering increases the dwell time of light in the active medium, enhancing stimulated emission. Moreover, as it will be discussed in the following, recurrent light scattering can provide a coherent feedback mechanism for laser oscillation. Lasing in disordered media has been a subject of intense theoretical and experimental studies from its first observations.

Just like in a regular laser it is the cavity that determines the modes, in a disordered gain media the modes are determined by multiple scattering. Light ampli-

fication is provided by stimulated emission but the feedback is supplied by scattering. Two different types of feedback were individuated for lasing in disordered media, one is an intensity feedback since it is incoherent and non-resonant, the other is a field feedback, coherent and resonant. Basing on the feedback mechanism involved, random lasers are thus classified as random lasers with incoherent feedback and random lasers with coherent feedback. Cao [11] and Wiersma [12], reviewed in detail the relevant physics, discussing both practical and potential applications of random lasers. Part of their discussion is summarized in the following section, with the aim to trace the evolution in the comprehension of random lasers, starting from the first experiments on the subject.

The first observation of an incoherent random laser was made by Ambartsumyan *et al.* in 1966 by replacing one mirror of a normal cavity with a scattering surface [13]. In this kind of cavity light experiences multiple scattering, changing its direction each time it is scattered by the surface. After one round trip, light does not return to its original position and, as a consequence, ordinary spatial resonances cannot form and the dwell time is independent on frequency. The feedback in such a laser consists only in bringing part of the energy back to the gain medium, that is, it is an energy feedback mechanism. The absence of resonant feedback results in an almost continuous emission spectrum, which does not contain discrete resonant frequencies. By increasing the pumping rate, the broad active medium emission spectrum undergoes a spectral narrowing around the frequency corresponding to the maximum of the gain [14]. This is the result of a non-resonant feedback mechanism, where instead of individual high-Q resonances, a large number of low-Q resonances appear, which overlap and form a continuous spectrum. The statistical properties of laser emission are quite different from those of an ordinary laser, and rather much closer to those of a black body in a narrow range of the spectrum [15].

In 1986 Markushev *et al.* reported intense stimulated radiation from neodymium in a polycrystalline powder of $Na_5La(MoO_4)_4$, under resonant pumping at low temperature (77 K) [16]. When the pumping intensity exceeded a threshold, the duration (140 μs) of the luminescence of the strongest emission component of Nd^{3+} transition ($\lambda \sim$1066 nm) reduced by about four orders of magnitude and its spectral width decreased to the instrumental width. In a powder of small particles (1-10 μm) with irregular shape there was only one narrow emission line at the centre of a luminescence band, while in a powder of bigger regularly shaped (20-

50 μm) particles the emission spectrum consisted of several lines in the range of the luminescence band [17]. In all cases, the spectral width of the emission lines above the threshold was on the order of 0.1 nm. The observed emission was very much like laser emission.

Other gain materials as Ti:sapphire powder [18], Pr^{3+}-doped powder [19] and LiF with color centres [20] were studied. Despite the different materials, common phenomena were observed such as the spectral narrowing of the emission line above a pumping threshold and a drastic shortening of the emission pulse, damped oscillation of the emission intensity under pulsed excitation, drifting of the stimulated emission frequency and hopping of the emission line from one discrete frequency to another within the same series of pulses. Gouedard *et al.* analyzed the spatial and temporal coherence of the powder laser [21], concluding that the emission of powders above the threshold is characterized by spatial incoherence and a low temporal coherence (~10 ps). The feedback mechanism was yet not fully understood, Gouedard *et al.* hypothesized that the grains of the powder emit collectively in a pulse where multiple scattering provides a distributed feedback.

Noginov *et al.* compared the powder laser with the single-crystal laser, observing that photon diffusion intervenes in the stimulated emission process, leading to longer paths in the powder and to a reduction of the threshold. To this purpose Wiersma & Lagendijk proposed a model based on light diffusion with gain [22]. They considered an incident pump pulse and probe pulse onto a powder slab. The active material was approximated as a four-level system – 2, 1, 0_a, 0_b – with the radiative transition from level 1 to 0_a and the pumping from level 0_b to 2. Fast relaxation from level 2 to 1 and from level 0_a to 0_b makes both level 2 and 0_a nearly unpopulated, thus the population of level 1 can be described by one rate equation. The whole system was described by three diffusion equations, they numerically solved the coupled nonlinear differential equations and the simulation result reproduced the experimental observation of transient oscillation of the emission intensity under pulsed excitation. In powders, the gain and scattering medium are not separated, and it is difficult to say if the feedback is provided by multiple scattering or total internal reflection, since both the models based on light diffusion [22] and intraparticle resonances [21] reproduced the experimental phenomena.

Lawandy *et al.* separated the scattering and gain media observing laser-like

emission from a methanol solution of rhodamine 640 perchlorate dye and TiO_2 particles, with a mean diameter of 250 nm, as scattering centers [23]. The peak of emission intensity reported versus the pump energy exhibited a well defined slope change. At that threshold, the emission linewidth collapsed rapidly from 70 to 4 nm, and the duration of emission pulses was shortened from 4 ns to 100 ps. The threshold behavior suggested the onset of a feedback mechanism, while the broad emission spectrum above the threshold indicated that the feedback was not resonant. When the density of scattering particles was increased from $5{\cdot}10^9$ to $2.5{\cdot}10^{12}\,cm^{-3}$ at the fixed dye concentration of $2.5{\cdot}10^{-3}$ M, it was found experimentally that the threshold was reduced by more than two orders of magnitude. This strong dependence of the threshold on transport mean free path revealed that the feedback was related to scattering [24, 25]. In these cases the gain medium extended exclusively outside the scatterers that were too small to work as resonators.

As explained in section 2.1, multiple scattering or light diffusion is negligible unless the dimension of the scattering medium is much larger than the transport mean free path. In the case of Lawandy's experiment the thickness of the entire suspension was much larger than the transport mean free path, so light transport in the suspension was diffusive. The emitted photons could escape from the small amplifying region toward the unpumped region of the sample or the air through the facet of the cell containing the solution. The remaining photons had a certain probability to return to the gain volume for further amplification by performing a random walk. The return probability increases, as well as the feedback, if scattering is stronger. The threshold for lasing is reached when the rate of losses is equal to the amplification rate.

The frequency dependence of gain ensures that the highest photon generation rate happens at the peak of the gain spectrum. On the other hand, the transport mean free path weakly depends on frequency, thus the feedback is nearly frequency independent within the gain spectrum, as well as the loss rate. By increasing the pumping rate, the photon generation rate in the spectral region of maximum gain first reaches the threshold, while in the outer spectral region the photon generation is lower than the loss rate. The photon density increases more and more around the frequency of the gain maximum, resulting in a collapse of the emission linewidth.

Balachandran, Lawandy and Moon proposed a model of random laser based

on the ring laser in the limit of random phase [26]. They used the Monte Carlo method to calculate the return probabilities of photons experiencing random walks and their average total path length. The amplifying volume was approximated with a disk of homogeneous gain coefficient. The threshold gain was determined by the steady-state condition, analogously to what is found for a ring laser. In the scattering medium the condition on round-trip phase shift (a multiple of 2π) that determines the lasing modes in a regular ring laser can not be considered. Since the feedback is non-resonant, in this case the requirement is simply that light returns to the gain volume and not necessarily to its original position. This assumption is always valid in the diffusive regime for a 3D medium, where the probability of light returning to its original position is so low that interference effects are totally negligible.

2.2.1 Emission properties of random lasers

Energy feedback random lasers Zhang *et al.* investigated the threshold for random lasing varying the dye concentration and the gain length. The threshold was reached when the pump transition was bleached. At bleaching, the penetration length of the pump increases, consequently emitted light travels a longer path inside the gain medium, resulting in a reduced threshold [28]. A similar consideration holds for the pump diameter, with a strong increase of the threshold pump intensity when reducing the illumination spot size [29]. When the excitation beam diameter is of the same order of the mean free path the threshold pump intensity increased by a factor of 70. This is because a large pump beam produces a large amplified region, providing higher amplification to the emitted photons. This also holds in the inward direction, indeed, as the probability of coming back from unpumped regions, for escaped photons, is larger for a bigger pumped volume. For small excitation beam diameters, the emitted light leaves the active volume after a short time, and also the chance of returning is small. This causes larger photon loss rate and therefore a higher threshold. The amplification by stimulated emission was found to be strongest when the absorption length of the pump light is of the same order of magnitude of the transport mean free path [30]. Totsuka *et al.* found a critical transport mean free path for each pump beam diameter, below which the threshold was almost independent of the mean free path [31]. These results can be explained in terms of the spatial over-

lap of the gain volume and the diffusion volume. When the gain volume, or in other words the spatial extent of the region containing the excited molecules, is smaller than the diffusion volume, the amplification is not efficient, since light propagates mostly through unpumped region. If the gain volume is larger than the diffusion volume for light, part of the excitation pulse is not employed in the amplification. The optimal condition is calculated in [31], by solving the coupled rate and diffusion equations.

van Soest & Lagendijk introduced, following the theory of traditional laser, the spontaneous emission coupling factor β for the random laser [32]. The factor β is defined as the ratio of the rate of spontaneous emission into the lasing modes to the total rate of spontaneous emission. Its value is determined by the overlap in the wavevector space between the spontaneous emission and laser field. While the spontaneous emission is isotropic, conventional cavity modes subtend thin solid angles, resulting in a very small contribution of spontaneous emission to the cavity modes ($\beta \sim 10^{-5}$). In the scattering medium, the diffusive feedback does not conserve directionality, thus the spatial distinction between lasing and non-lasing modes vanishes, and the only criterion is the spectral overlap of the spontaneous emission spectrum with the lasing spectrum. This gives a large β value ~0.1.

Coherent feedback random lasers In 1998 Cao *et al.* observed a different kind of lasing process in disordered semiconductor powders [34] and polycrystalline films [33], where the feedback was frequency dependent, and supplied by recurrent light scattering (i.e. multiple scattered light returns to a scatterer from which it has been scattered before). Similar lasing phenomena were also observed in luminescent π-conjugated polymer films [35], organic dye-doped gel films [36], opal crystals saturated with polymer and laser dye solutions [37]. This kind of lasing phenomenon was called random laser with coherent feedback.

Cao *et al.* made their experiment with polydisperse ZnO nanoparticles with an average particle size of 100 nm and a filling factor around 50%, deposited onto an ITO-coated substrate [33]. The sample thickness varied from 10 μm to 1 mm. The ZnO samples were optically excited by picosecond pulses of third harmonic and fourth harmonic of a Nd:YAG laser. The pump beam was focused on the sample surface, the electrons in the ZnO valence band absorbed pump photons and jumped to the conduction band. They subsequently relaxed to the bottom of the

conduction band before radiative decay. At low excitation intensity, the spectrum consisted of a single broad spontaneous emission peak. As the pump power increased, the emission peak became narrower owing to preferential amplification at frequencies close to the maximum of the gain spectrum. When the excitation intensity exceeded a threshold, discrete narrow peaks emerged in the emission spectra. The linewidth of these peaks was less than 0.2 nm, 30 times narrower than the linewidth of the amplified spontaneous emission (ASE) peak below the threshold. When the pump intensity increased further, even sharper peaks appeared, whose frequencies depended on the position of the excitation spot on the sample. This phenomenon suggests that the discrete spectral peaks are the result of the interference of scattered waves in the ZnO powder, so it is related to the configurations of ZnO particles. The probability of intra-particle resonances formed by total internal reflection at the particle surfaces can be excluded since the single ZnO nanoparticles are too small to serve as resonators. Thus the origin of the spatial resonances lies in the inter-particle scattering. When scattering is strong enough to give rise to recurrent scattering events, interference of return light becomes constructive only at certain frequencies. Therefore, the requirement for constructive interference of backscattered light selects the resonant frequencies. A threshold behavior was observed: above the pump intensity at which discrete spectral peaks emerged, the emission intensity increased much more rapidly with the excitation intensity. Light can be trapped in these regions through multiple scattering and interference. For a particular configuration of ZnO nanoparticles, only light at certain frequencies can be confined, because the interference effect is frequency sensitive. In a different region of the sample, the particle configuration is different, thus light at different frequencies is confined. In other words, there are many resonant cavities formed by recurrent scattering and interference. Incomplete trapping of light gives rise to cavity loss. When the optical gain reaches the cavity loss, laser oscillation occurs in the cavity modes, that gives discrete lasing peaks in the emission [11].

The statistical property of the emissions from ZnO powder was probed by Cao *et al.* using a streak-camera in the photon counting mode [38]. They selected the spectral interval corresponding to an emission peak, and counted the photons for each pulse. After collecting photon count data for a large number of emissions where discrete spectral peaks appear, the probability $P(n)$ of detecting n

photons in the wavelength interval $\Delta\lambda$, is obtained for the single modes [1].

Below threshold the measured photon count distribution was almost identical to the Bose-Einstein (BE) distribution, the same of a chaotic light source. As the pump intensity was increased the photon statistics of ZnO emission started deviating from the BE statistics, when the pump intensity was slightly above the threshold, the measured photon count distribution was between a BE distribution and the Poisson distribution. When the pump intensity was 6 times the threshold, the photon count distribution was nearly identical to the Poisson distribution. The photon statistics of the random laser with coherent feedback is therefore similar to that of a traditional laser, and different from the photon statistics of the random laser with incoherent feedback, which is a linear superposition of coherent and incoherent components, as observed by Zacharakis *et al.* [39]. In their non-resonant random laser, above threshold, the coherent component reached a plateau of 51% of the emitted light.

2.2.2 Random laser with dye solutions

The previous section illustrates that the behavior of the random laser with coherent feedback is quite different from that of the random laser with incoherent feedback. To understand this difference, Cao *et al.* studied the transition between them by varying the amount of scattering in the gain medium [40]. The random media used in this experiment were rhodamine 640 dye solutions containing ZnO nanoparticles. The advantage of the solutions was that the scattering length can be varied continuously by changing the density of scatterers in the solutions. A pulsed picosecond Nd:YAG laser was used to excite the dye molecules in the solution. The emission spectrum was captured after a single pump pulse. The evolution of the emission spectra by varying the pump intensity is observed, whit a particle density of $2.5{\cdot}10^{11}$ cm^{-3} and a dye concentration of 5 mM. When the pump intensity crossed a threshold, a drastic spectral narrowing occurred. Once above the threshold, the emission linewidth collapsed to ~5 nm. Simultaneously, the peak emission intensity increased dramatically. This phenomenon was identical to that observed by Lawandy *et al.*, [23]. It corresponded to lasing

[1] For single-mode coherent light, the photon number distribution $P(n)$ satisfies the Poisson distribution, $P(n) = \frac{\langle n\rangle^n e^{-\langle n\rangle}}{n!}$ For single-mode chaotic light, the photon number distribution $P(n)$ satisfies the Bose-Einstein (B-E) distribution, $P(n) = \frac{\langle n\rangle^n}{[1+\langle n\rangle^n]}$.

with non-resonant feedback occurring in the colloid [23]. An analogous result is reported as example in Figure 2.1 for an ethanol solution of dye (Rhodamine 6g) and TiO_2 nanoparticles.

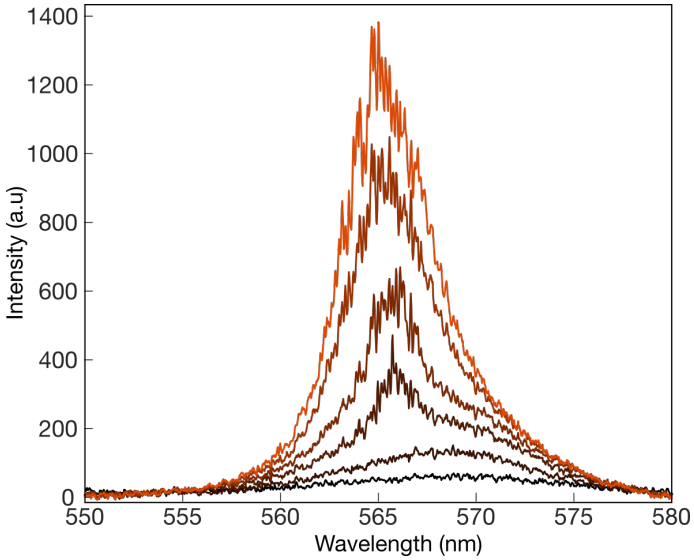

Figure 2.1: Emission spectra of a 5mM solution of Rhodamine 6g and ethanol, with a scatterer concentration of $\sim 10^9$ cm^{-3}, when the pump excitation is varied from 0.5 µJ to 5 µJ. The pump laser is a frequency-doubled Nd:YAG pulsed laser (20 ps).

When the particle density was increased from to $2.5{\cdot}10^{11}$ cm^{-3} to $5{\cdot}10^{11}$ cm^{-3}, keeping the dye concentration constant, two thresholds were observed [40]. The first threshold corresponded to the spectral narrowing until 5 nm. If pump intensity was increased further, a second threshold was reached, where discrete spectral peaks of linewidth $\lesssim 0.2$ nm emerged on the gain curve. This phenomenon was very similar to what observed in the ZnO powder [33] and corresponds to lasing with coherent feedback. In this case the frequencies of the lasing modes are different for each pump pulse. When the ZnO particle density was increased to $1{\cdot}10^{12}$ cm^{-3} the discrete spectral peaks appeared before the collapse of the emission linewidth, indicating that the threshold for lasing with coherent feedback became lower than the threshold for lasing with incoherent feedback in the strong scattering medium (exemplary spectra showing this phenomenon are reported in Figure 2.2).

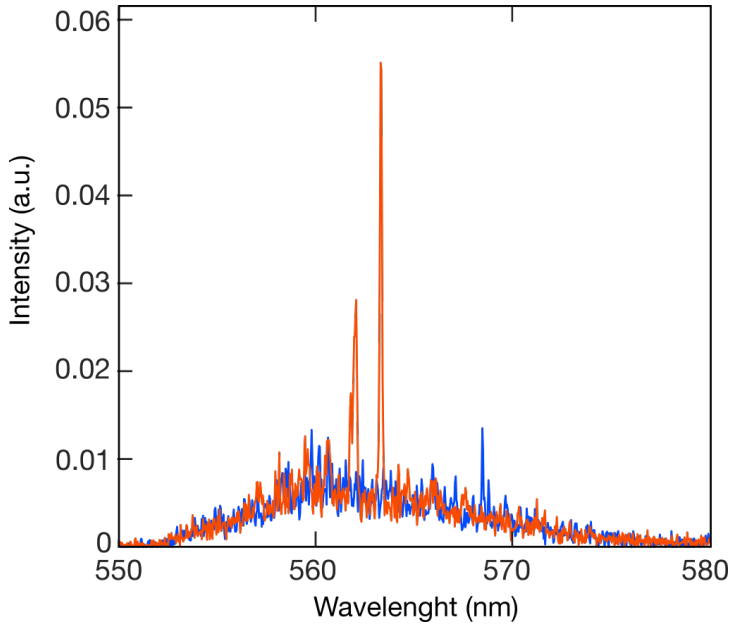

Figure 2.2: Two exemplary emission shots at threshold crossing from an ethanol solution of 5mM of Rhodamine 6G and a scatterer concentration of $\sim 10^{12}$ cm^{-3}. The blue curve shows the emission below threshold. Narrow peaks of linewidth of less than 0.2 nm appear upon the gain curve, before observing spectral narrowing of the gain curve (orange curve).

Transition between the feedback mechanisms The above phenomena was explained directly by Cao in terms of Maxwell equations in a random medium [11]. Since the random medium can be seen as an open system with finite size, its modes can be therefore described with complex eigenenergies with the imaginary parts representing the decay rates. The coupling to the outside reservoir (the modes outside the random medium) makes modes interact with each other, meaning that photons of one mode can hop to another one through scattering at the boundary. In the regime of non-localization for light, the average decay rate of an eigenmode is larger than the mean frequency spacing of adjacent modes. Then, the eigenmodes are spectrally overlapped resulting in a continuous emission spectrum. When scattering is weak, the coupling between the modes is stronger. Due to photon exchange among the modes, the photon loss rate for a set of interacting modes is much lower than that of a single mode. At the frequency of maximum gain, when the optical gain for a set of interacting modes reaches the threshold, the total photon number in these coupled modes grows, giving origin to the phenomenon of lasing with incoherent feedback. The increase of photon number at the frequency of gain maximum determines a spectral narrowing. Well above the threshold, gain saturation quenches the total photon number fluctuation. When modes are strongly coupled, photon hopping occurs, preventing the stabilization of the photon number in a single mode. If the dwell time of light in the random medium increases, for example by increasing the amount of optical scattering, the coupling of the modes with the external reservoir is weakened, consequently the interaction among the modes is lower. When the optical gain increases, a set of coupled modes at the frequency of gain maximum firstly reaches the threshold for lasing, and when the optical gain increases further, the single mode with longer lifetime finally reaches the threshold and lasing occurs in this mode. A further increase of optical gain leads to lasing also in other modes with low losses. These conditions give origin to discrete peaks in the emission spectrum. When the scattering strength increases further, the decay rates of the eigenmodes and the coupling among them continue to decrease. There are few eigenmodes with long lifetimes which are nearly decoupled from the others. As a result, the threshold for lasing in these individual modes becomes lower than the threshold gain for lasing in a set of coupled modes and lasing occurs even before spectral narrowing of the ASE is reached. Above the threshold, because of weak coupling between the modes, the fluctuation of the

photon number in each mode is quenched by the gain saturation effect, while in a random laser with incoherent feedback is rather the total number of photons in all the modes to be suppressed by gain saturation.

Intensity fluctuations When lasing occurs in a large number of strongly coupled modes, the sensitivity to the boundary conditions is higher. In a pulsed configuration, the random laser can show a chaotic behavior in its temporal and spectral response, meaning that each time the medium is excited, if there is no specific frequency dominating the others, the laser shots exhibit different spectra [12]. One could think that the reason for the observation of uncorrelated laser spectra in a dye solution with suspension of scattering nanoparticles is due to motion of particles inside a liquid that change continuously their configurations, however this is not the case. Mujumdar *et al.* performed an experiment with Rhodamine 6G infiltrated inside a porous glass, i.e. in a configuration where the active medium is embedded in a random material with static disorder, and they also observed distinct random laser shots totally different from each other [41]. It was found that the narrow emission spikes in the emission spectrum can change frequency in a random fashion from one excitation pulse to another. This chaotic behavior is observed under the specific conditions of fast excitation source (tens of picoseconds) and by collecting single-shot emission spectra. Additionally, the threshold of a random-laser system can also show chaotic behavior, in the sense that under repeatable experimental conditions the system jumps above and below threshold [42]. This can be explained again with the high sensitivity of the system to small intensity fluctuations [43]. The consequence of these fluctuations is that the intensity distribution obeys a Lévy type statistic. The Lévy distribution belongs to the family of stable distributions, it is characterized by an infinite variance, since the occurrences of rare but very large values contributes to a slowly decaying tail (see Appendix A). It was found that there exist three different regimes for the laser intensity fluctuations: the threshold where Lévy statistic applies, and below and above the threshold where the statistics remain gaussian [44–46]. The Lévy regime corresponds to the range where spectra have an accentuated chaotic character.

Linewidth and peak frequency tuning Most of the characteristics of random lasers realized with dye solutions and scattering particles, are also on average

applicable to a vast variety of active media and disordered matrices from which random lasers can be realized. One of the appealing characteristic of the random laser is its narrow linewidth. Tuning the linewidth of random lasers is crucial to promote their practical applications. However, the disordered structures make this tuning very complex. To date, how to realize a random laser with tunable linewidth or increasingly narrow lines is a relevant challenge. Our novel technique presented and explained in detail in Chapters 4 and 5 of super-resolved spectral reconstruction requires narrow laser linewidths to improve the resolution. In accordance with what we discussed in the previous sections, random lasing with a line width of few nanometers is considered to be the result of incoherent feedback (see Figure 2.1) while coherent feedback leads to narrower peaks with sub-nanometer width (see Figure 2.2). Experimentally, by tuning the composition of the random laser, such as the concentrations of scatterers and the gain material, as well as the pumping area, the switch between these two regimes can be achieved as desired [40]. However, an optimization of the linewidth needs still to be reached, and constitutes an open issue. In recent years many works in this direction were presented, for example the manipulation of plasmonic scattering of metal particles with plenty of nanogaps is proposed as an effective method to achieve line width-tunable random lasers from 0.03 to 6.5 nm, with a tuning range exceeding 2 orders of magnitude [47].

Similar results were obtained also for the tuning of the emission lines, a multicolor coherent random laser using various laser dyes, based on cascade energy transfer, was developed [48]. Moreover, Bachelard *et al.* showed experimentally that control over emission can be gained by actively shaping the optical pump inside the random laser, and single-mode operation at any selected wavelength can be achieved with spectral selectivity down to 0.06 nm [49]. This method opens the way towards versatile tunable and controlled random lasers, with ultra-narrow emission lines (~0.03 nm).

2.3 Optimization and application of random lasers

The peculiar properties of random laser, also benefitting from low cost and robustness of operation finds a lot of potential and practical applications in many different fields. For example, the low coherence of random lasers with incoherent

feedback which translates into a low contrast speckle pattern, is very attractive for applications requiring high uniformity of the field distribution. They can be advantageous in holography, in the energy transport in fibers for medical applications, and generally in all applications where the coherent properties of conventional lasers represent a disadvantage as they would degrade luminescence uniformity. Redding *et al.* exploited the low spatial coherence of specifically designed random lasers to demonstrate speckle-free full-field imaging in the setting of intense optical scattering [2]. They quantitatively showed that images generated with random laser illumination exhibit superior quality than images generated with spatially coherent illumination. Recently, a random laser has been exploited in optical sensing applications. By maintaining the active medium separated from the diffusive one Ignesti *et al.* built a self-contained optical sensor that could be employed in non-invasive diagnostics of biological samples [50]. Random lasers however are notorious for their unpredictability, with large efforts being dedicated to obtaining at least a partial control of their emission properties. Lee *et al.* experimentally observed that photonic band-tail eigenstates, which are manifestations of photonic Anderson localizations, are responsible for random lasing in a compositionally disordered photonic crystal [51]. They also demonstrated that the process of governing the band-tails offers an opportunity to regulate random laser emissions [52].

For all the mentioned applications, from sensing and spectroscopy to speckle-free imaging, it is moreover useful to have high-radiance sources operating in continuous-wave (CW). Biasco *et al.* demonstrated the CW operation of a random laser using an electrically pumped quantum-cascade laser gain medium in which a bi-dimensional random distribution of air holes is patterned into the top metal waveguide [53]. They obtained a highly collimated vertical emission at 3 THz and CW emission of 1.7 mW. An external cavity formed with a movable mirror was used to tune the random laser over 11 GHz.

As concerns the random laser efficiency, many different kind of lasing mechanisms have been proposed in the latest two years. Wu *et al.* studied random lasing in a metal surface plasmon waveguide with gold-plated silicon pyramids. The emission efficiency of the random laser was greatly enhanced through the spiky tips. The surface plasmon waveguide confined the emitted light in a certain direction with a small divergence angle. They found that the enhancement effect for the random laser is likely to be due to the localized surface plasmon

(LSP) field. The LSP field nearby the spiky tips can enhance field-molecule interaction, which is beneficial for lasing at small scale, opening the way for the application of random lasers in sub-wavelength optical elements [54].

However, as remarked by Yu in his review, for random lasers to be useful, electrical excitation (i.e. the realization of laser diodes) is an essential condition for commercialization [55]. It is necessary to overcome the problems of high scattering loss and multidirectional emission from the random media. If these requirements can be fulfilled, random lasers will provide the ideal light sources for laser projectors, spotlights, car headlights, etc. A random laser diode can simultaneously offer compact size, low power consumption and collimated incoherent emission. Nevertheless, the development of electrically pumped random lasers is still in its infancy. A recent demonstration of an electrically-pumped random laser was made in 2013 by Liang *et al.* They realized for the first time a random laser in the mid-IR regime, using a random distribution of air holes patterned on quantum cascade laser heterostructures (GaAs/InAlAs)[56]. For a sufficiently dense configuration of air holes, random peaks arise due to multiple scattering and interference, and either multi-peak or single lasing regime can be switched depending on the size of the structure. The proposed method provides a platform for studying the physics of random lasing with controllable randomness, and further prove that random lasing can be observed at a wide range of wavelengths and in a broad range of material system.

The proposal of using GaAs- and GaN-based materials for the fabrication of random laser diodes might be the most promising, since the design and fabrication technologies of GaAs- and GaN-based double hetero-structures is well established and commercially available. The problems of high scattering losses and multidirectional emission can be suppressed by using a waveguide design. Moreover, the unexplored nonlinear processes at the basis of random laser diodes makes the development of functional electrically driven random lasers even more interesting.

References

1. Ghofraniha, N. *et al.* Experimental evidence of replica symmetry breaking in random lasers. *Nature Communications* **6,** 6058 (Jan. 2015).

2. Redding, B., Choma, M. A. & Cao, H. Speckle-free laser imaging using random laser illumination. *Nature photonics* **6,** 355–359 (2012).

3. Tureci, H., Ge, L., Rotter, S. & Stone, A. Strong Interactions in Multimode Random Lasers. *Science (New York, N.Y.)* **320,** 643–6 (June 2008).

4. Van der Molen, K. L., Tjerkstra, R. W., Mosk, A. P. & Lagendijk, A. Spatial Extent of Random Laser Modes. *Phys. Rev. Lett.* **98,** 143901 (14 Apr. 2007).

5. John, S. Localization of Light. *Physics Today* **44,** 32–40 (1991).

6. Bohren, C. F. & Huffman, D. R. *Absorption and scattering of light by small particles* 530 (Wiley, 2004).

7. Kuga, Y. & Ishimaru, A. Retroreflectance from a dense distribution of spherical particles. *J. Opt. Soc. Am. A* **1,** 831–835 (1984).

8. Albada, M. P. V. & Lagendijk, A. Observation of Weak Localization of Light in a Random Medium. *Phys. Rev. Lett.* **55,** 2692–2695 (24 1985).

9. Wolf, P.-E. & Maret, G. Weak Localization and Coherent Backscattering of Photons in Disordered Media. *Phys. Rev. Lett.* **55,** 2696–2699 (24 1985).

10. Abrahams, E., Anderson, P. W., Licciardello, D. C. & Ramakrishnan, T. V. Scaling Theory of Localization: Absence of Quantum Diffusion in Two Dimensions. *Phys. Rev. Lett.* **42,** 673–676 (10 1979).

11. Cao, H. Lasing in random media. *Waves in Random Media* **13,** R1–R39 (2003).

12. Wiersma, D. S. The physics and applications of random lasers. *Nature Physics* **4,** 359–367 (2008).

13. Ambartsumyan, R., Basov, N., Kryukov, P. & Letokhov, V. Non-resonant feedback in lasers. *Progress in Quantum Electronics* **1,** 107–185 (Jan. 1970).

14. Ambartsumyan, R. V., Basov, N. G., Kryukov, P. G. & Letokhov, V. S. A laser with nonresonant feedback. *Soviet Physics JETP* **24,** 724–729 (1967).

15. Ambartsumyan, R., Basov, N. & Letokhov, V. Statistical Emission Properties of a Nonresonant Feedback Laser. *Soviet Journal JETP* **53,** 1109 (1968).

16. Markushev, V. M., Zolin, V. F. & Briskina, C. M. Luminescence and stimulated emission of neodymium in sodium lanthanum molybdate powders. *Soviet Journal of Quantum Electronics* **16,** 281–283 (1986).

17. Ter-Gabriélyan, N. É. *et al.* Stimulated radiation emitted by lithium neodymium tetraphosphate LiNd (PO3)4and neodymium pentaphosphate NdP5O14powders. *Soviet Journal of Quantum Electronics* **21,** 840–842 (1991).

18. Noginov, M. *et al.* Study of the pumping regimes in Ti-sapphire and Nd0.5La0.5Al3(BO3)4 powders. *Optical Materials* **10,** 297–303 (1998).

19. Zolin, V. The nature of plaser-powdered laser. *Journal of Alloys and Compounds* **300-301,** 214–217 (2000).

20. Noginov, M. A. *et al.* Color-center powder laser: the effect of pulverization on color-center characteristics. *J. Opt. Soc. Am. B* **14,** 2153–2160 (Aug. 1997).

21. Gouedard, C., Husson, D., Sauteret, C., Auzel, F. & Migus, A. Generation of spatially incoherent short pulses in laser-pumped neodymium stoichiometric crystals and powders. *J. Opt. Soc. Am. B* **10,** 2358–2363 (Dec. 1993).

22. Wiersma, D. S. & Lagendijk, A. Light diffusion with gain and random lasers. *Physical Review E* **54,** 4256–4265 (Oct. 1996).

23. Lawandy, N. M., Balachandran, R. M., Gomes, A. S. L. & Sauvain, E. Laser action in strongly scattering media. *Nature* **368,** 436–438 (1994).

24. Sha, W. L., Liu, C.-H. & Alfano, R. R. Spectral and temporal measurements of laser action of Rhodamine 640 dye in strongly scattering media. *Opt. Lett.* **19,** 1922–1924 (1994).

25. Zhang, W., Cue, N. & Yoo, K. M. Emission linewidth of laser action in random gain media. *Opt. Lett.* **20,** 961–963 (1995).

26. Balachandran, R. M., Lawandy, N. M. & Moon, J. A. Theory of laser action in scattering gain media. *Opt. Lett.* **22,** 319–321 (Mar. 1997).

27. Zhang, D. *et al.* Narrow-bandwidth emission from a suspension of dye and scatterers. *Optics Communications* **118,** 462–465 (1995).

28. Siddique, M., Alfano, R. R., Berger, G. A., Kempe, M. & Genack, A. Z. Time-resolved studies of stimulated emission from colloidal dye solutions. *Opt. Lett.* **21,** 450–452 (Apr. 1996).

29. Van Soest, G., Tomita, M. & Lagendijk, A. Amplifying volume in scattering media. *Opt. Lett.* **24,** 306–308 (Mar. 1999).

30. Beckering, G., Zilker, S. J. & Haarer, D. Spectral measurements of the emission from highly scattering gain media. *Opt. Lett.* **22,** 1427–1429 (Sept. 1997).

31. Totsuka, K., van Soest, G., Ito, T., Lagendijk, A. & Tomita, M. Amplification and diffusion of spontaneous emission in strongly scattering medium. *Journal of Applied Physics* **87,** 7623–7628 (2000).

32. Van Soest, G. & Lagendijk, A. β factor in a random laser. *Phys. Rev. E* **65,** 047601 (4 Mar. 2002).

33. Cao, H. *et al.* Ultraviolet lasing in resonators formed by scattering in semiconductor polycrystalline films. *Applied Physics Letters* **73,** 3656–3658 (Dec. 1998).

34. Cao, H. *et al.* Random Laser Action in Semiconductor Powder. *Physical Review Letters* **82,** 2278–2281 (Mar. 1999).

35. Frolov, S., Shkunov, M., Fujii, A., Yoshino, K. & Vardeny, Z. Lasing and stimulated emission in /spl pi/-conjugated polymers. *IEEE Journal of Quantum Electronics* **36,** 2–11 (Jan. 2000).

36. Frolov, S. V., Vardeny, Z. V., Yoshino, K., Zakhidov, A. & Baughman, R. H. Stimulated emission in high-gain organic media. *Physical Review B* **59,** 5284–5287 (Feb. 1999).

37. Yoshino, K. *et al.* Amplified spontaneous emission and lasing in conducting polymers and fluorescent dyes in opals as photonic crystals. *Applied Physics Letters* **74,** 2590–2592 (1999).

38. Cao, H., Ling, Y., Xu, J. Y., Cao, C. Q. & Kumar, P. Photon Statistics of Random Lasers with Resonant Feedback. *Phys. Rev. Lett.* **86,** 4524–4527 (20 2001).

39. Zacharakis, G., Papadogiannis, N. A., Filippidis, G. & Papazoglou, T. G. Photon statistics of laserlike emission from polymeric scattering gain media. *Opt. Lett.* **25,** 923–925 (June 2000).

40. Cao, H., Xu, J. Y., Chang, S.-H. & Ho, S. T. Transition from amplified spontaneous emission to laser action in strongly scattering media. *Phys. Rev. E* **61,** 1985 (2000).

41. Mujumdar, S., Türck, V., Torre, R. & Wiersma, D. S. Chaotic behavior of a random laser with static disorder. *Phys. Rev. A* **76,** 033807 (Sept. 2007).

42. Anglos, D. *et al.* Random laser action in organic–inorganic nanocomposites. *Journal of the Optical Society of America B* **21,** 208 (Jan. 2004).

43. Van der Molen, K. L., Mosk, A. P. & Lagendijk, A. Intrinsic intensity fluctuations in random lasers. *Physical Review A* **74,** 053808 (Nov. 2006).

44. Uppu, R., Tiwari, A. K. & Mujumdar, S. Identification of statistical regimes and crossovers in coherent random laser emission. *Optics Letters* **37,** 662 (Feb. 2012).

45. Uppu, R. & Mujumdar, S. Lévy exponents as universal identifiers of threshold and criticality in random lasers. *Phys. Rev. A* **90,** 025801 (2 2014).

46. Sharma, D., Ramachandran, H. & Kumar, N. Lévy statistics of emission from a novel random amplifying medium: an optical realization of the Arrhenius cascade. *Optics Letters* **31,** 1806 (June 2006).

47. Shi, X., Chang, Q., Bian, Y., Cui, H. & Wang, Z. Line Width-Tunable Random Laser Based on Manipulating Plasmonic Scattering. *ACS Photonics* **6,** 2245–2251 (2019).

48. Shi, X. *et al.* Random Lasing with a High Quality Factor over the Whole Visible Range Based on Cascade Energy Transfer. *Advanced Optical Materials* **2,** 88–93 (2014).

49. Bachelard, N., Gigan, S., Noblin, X. & Sebbah, P. Adaptive pumping for spectral control of random lasers. *Nature Physics* **10,** 426–431 (2014).

50. Ignesti, E. *et al.* A new class of optical sensors: A random laser based device. *Scientific Reports* **6** (2016).

51. Lee, M. *et al.* Anderson localizations and photonic band-tail states observed in compositionally disordered platform. *Science Advances* **4** (2018).

52. Lee, M., Callard, S., Seassal, C. & Jeon, H. Taming of random lasers. *Nature Photonics* **13,** 445–448 (2019).

53. Biasco, S. *et al.* Frequency-tunable continuous-wave random lasers at terahertz frequencies. *Light: Science & Applications* **8,** 43 (2019).

54. Wu, Y. *et al.* Enhanced random laser by metal surface-plasmon channel waveguide. *Opt. Express* **26,** 17511–17518 (2018).

55. Yu, S. F. Electrically pumped random lasers. *Journal of Physics D: Applied Physics* **48,** 483001 (2015).

56. Liang, H. K. *et al.* Electrically Pumped Mid-Infrared Random Lasers. *Advanced Materials* **25,** 6859–6863 (2013).

Chapter 3

Fabry-Pérot-like resonances in weakly scattering medium with gain

3.1 Introduction

As we have seen in Chapter 2 a feedback mechanism is required to achieve lasing oscillation: in a conventional laser it is provided by the mirrors and lasing occurs only via the modes that are defined by the geometry of the cavity. In a scattering medium with gain, recurrent scattering events provide amplification along closed loops that act as ring cavities for light, so that the modes associated to these random ring cavities can sustain lasing oscillations. When the scattering is weak, light performs a random walk with a vanishing probability of returning to a specific scatterer, then recurrent mechanisms can be neglected and in principle no kind of coherent feedback is typically achieved. However, lasing with coherent feedback can be still observed in many weakly scattering systems ranging from conjugated polymer films to organic dyes-doped gel films [1, 2], polymer-infiltrated opal crystals [3, 4] and laser dye solutions [5].

Polson *et al.* observed a certain degree of periodicity in the emission spectra associated with a coherent feedback signature, which was confirmed by a clear peak in the Fourier Transform spectrum as in the case of a laser resonator [4]. Wu *et al.* in 2006 performed a rigorous series of experiments on a colloidal suspension of scattering nanoparticles embedded in either diethylene glycol or methanol dye solutions [6]. Above a threshold pump intensity they observed nar-

row peaks (~ 0.1 nm wide) rising upon the gain medium curve (~20 nm wide), whose frequencies changed from shot to shot. Despite the fact that the frequencies of the peaks were uncorrelated among the shots, many spectra exhibited a resonator-like, constant frequency spacing of the lasing peaks. This constant frequency spacing can be interpreted with the free-spectral range of a standard Fabry-Perot cavity, whit the wavelength spacing $\Delta\lambda$ inversely proportional to the cavity length L_c:

$$\Delta\lambda = \frac{\lambda^2}{2nL_c} \tag{3.1}$$

where n is the effective refractive index. The estimated cavity length was $Lc \sim 200$-300 μm. The emission from the random laser sample was detected in the backward direction with respect to pump illumination. Images collected at 90° from the pump beam showed the lateral section of the excited volume revealing its conical shape, with the base at the cuvette entrance and the vertex inside the liquid solution. Since these systems were weakly scattering and the scattering mean free path was longer than the absorption length even at saturation condition, the cone shape was mainly determined by absorption and its height associated to the penetration length of the pump light inside the sample. The measured value of the cone height was comparable to the cavity length estimated from the regular spacing of the random laser peaks in the emission, suggesting an explanation for the comb-like resonances. Even if the feedback provided by scattering was weak, the high gain due to intense pumping was enough to create a coherent feedback effect, that resulted in narrow and discrete lasing peaks. Numerical calculations were showed sustaining the hypothesis that the major feedback to the observed Fabry-Perot like emissions was provided by particles at the boundaries of the pumped volume: two particles, respectively at the vertex, and at the base of the light cone, are sufficient to instaurate a resonant feedback. Indeed, the backscattered light from a scatterer at the boundaries of the pumped volume experiences an higher amplification than light scattered from particles in the central zone, which could explain why the mean cavity length retrieved from the periodic spectra was similar to the height of the cone. The authors associated the lasing phenomenon to that of a distributed feedback laser (DFBL) in undercoupling regime of operation, where the distributed feedback was provided by the random scattering particles inside the pumped volume, rather than from a periodic variation of the permittivity.

While the hypothesis of scattering particles can be considered reasonable in explaining the regular spacing between the peaks in the emission shots, the optical system used to image the liquid sample in their experiments did not have enough resolution to detect particle sizes of the order of few micrometers. Moreover, the images reproducing the light cone inside the sample were the result of an average over ~ 30 frames. The average precluded the possibility of studying the dynamic of the liquid, first of all the motion of the scattering particles. Since the scattering particles are fundamental for the formation of the regular resonances in the emissions, a synchronous acquisition between the single-shot spectra and the images of the sample at the same instants is necessary to look into this mechanism. In this work we present a detailed experimental study conducted on the random laser emissions from liquid weakly scattering dye solutions, by achieving triggered acquisitions of the sample images with the random laser pulses. These allows to investigate the importance of the contemporary presence of two scattering particles one in the vertex and one on the basis of the pumped volume and if this condition is sufficient to achieve a coherent feedback for random lasing.

3.2 Experimental results

In the following section we describe the random laser sample and the optical setup that we used to characterize the random laser emission. The weakly scattering systems consist of scattering nanoparticles of TiO_2 suspended in a solution of Rhodamine 6g and ethanol. The experiments were performed with various dye concentrations, 5 mM, 15 mM and 45 mM, and also particle density was varied from $3{\cdot}10^9$ to $8{\cdot}10^{10}$ cm^{-3} for a fixed dye concentration. The liquid sample contained in a cuvette was optically excited at λ= 532 nm by a Nd:YAG mode-locked laser with 20 ps pulse width and a repetition rate of 10 Hz. Figure 3.1 shows a scheme of the experimental setup. The pump beam was focused by a 10× objective lens into the solution through the front window of the cuvette. The light emitted in the backward direction is collimated by the same objective lens and focused with a second lens (f = 50 mm) into an optical fiber. The fiber output is focused at the entrance slit of a spectrometer and a CMOS camera triggered with the pump pulse records the single random laser emission shots, with a spectral

resolution of ~ 0.1 nm. An objective lens (20×, 0.5 NA) is placed in front of the cuvette, at 90° with respect to the pump beam producing a magnified image of the lateral emission which is detected by a second CMOS camera, synchronous with the pump pulse. Therefore, for each random laser emission shot we collect both its spectrum and a side image of the liquid sample. A white spectrum lamp was placed in the vicinity of the cuvette, orthogonal to the pump beam in order to create a diffuse illumination of the liquid. In this way the white light scattering from small TiO_2 particles or clusters makes them more visible inside the liquid. The characterization of the pump was performed by imaging the fluorescence signal emitted by a weakly absorbing $5{\cdot}10^{-6}$M solution of dye and ethanol (see Figure 3.1.b). The estimated focal spot of the pump is 10 μm.

Figure 3.2.a shows the ASE emission spectrum from a solution of 5mM dye in ethanol exhibiting characteristic resolution-limited spikes, over the large dye emission. The peaks in the ASE spectrum change stochastically their positions for different shots. The ASE emission has been fully explained in early works since its first observation [7–9]. The random spikes on the ASE spectrum originate from intensity fluctuations in time within the same ASE pulse and they average out when integrating over few shots. The time fluctuations are due to amplification of spontaneous emission mainly occurring along the direction of largest gain, and determined by the direction of maximum spatial extent of the pumped volume. In our case it assumes the shape of the gaussian beam penetrating inside the absorptive liquid medium.

Figure 3.2.b shows a random laser shot emission from a 5mM dye solution with a TiO_2 particle concentration of 10^9 cm^{-3}, the narrow discrete peaks with a width < 0.2 nm are uncorrelated among different emission shots. The shape and the origin of these peaks are different from the spikes rising on the ASE curve, where a coherent feedback mechanism intervenes to select narrow, discrete and highly prominent peaks that deplete the gain curve.

The singular characteristic of the shot of Figure 3.2.b is the regular spacing between the peaks within the spectrum, different from a typical random laser emission where peaks arise at unpredictable frequencies. This is also clearly shown by the peak in the Fourier Transform (Figure 3.2.d). Considering a statistical ensamble of thousands of shots, roughly 30% show this characteristic. In this subset, the absolute position of the peaks varies in a random fashion from shot to shot, but their relative spacing is almost constant ($\Delta\lambda \sim 0.4$ nm), with a relative standard

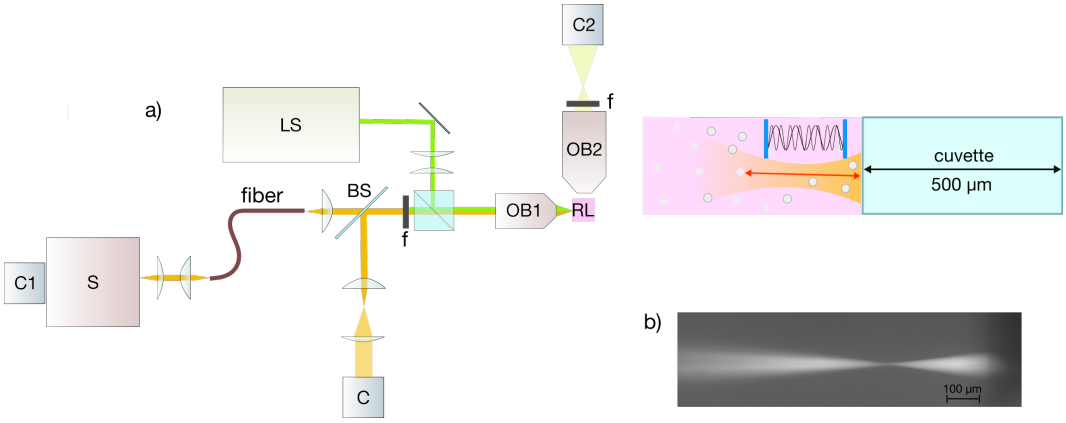

Figure 3.1: a) Scheme of the experimental setup. The random laser (RL) is optically excited by a pump laser (LS) which is focused using a 10× microscope objective (OB1). The same objective collimates the backscattered signal and the pump light is filtered out by an interference filter (f). Using a 50-50 beam splitter (BS), 50% the emission is focused to a multimodal fiber and then focused at the entrance of the spectrometer (S) and collected by a camera (C1). The rest is directed to a camera (C) in order to characterize the angular emissions. An other objective (OB2) is placed at ninety degrees with respect to the RL excitation beam. The images of the spatial characteristic of amplified spontaneous emission shots are collected by another camera (C2) synchronized with that placed at the spectrometer output. Then to each RL emission spectrum we can relate an image of the liquid sample at the same instant. The inset shows a graphical picture of the random laser sample and the cross-section of the cuvette wall (thickness ~ 500 µm). The sample is a solution of Rhodamine 6G and ethanol with a suspension of scattering TiO_2 nanoparticles. The picture is not to scale to highlight the effective cavities length inside the sample (200–300 µm), from the scattering particle to the inner face of the cuvette. b) The image shows the pump beam propagating in a weakly absorbing dye solution in ethanol. From this image we can estimate a focus waist of 10 µm). The right side shows part of the cuvette wall.

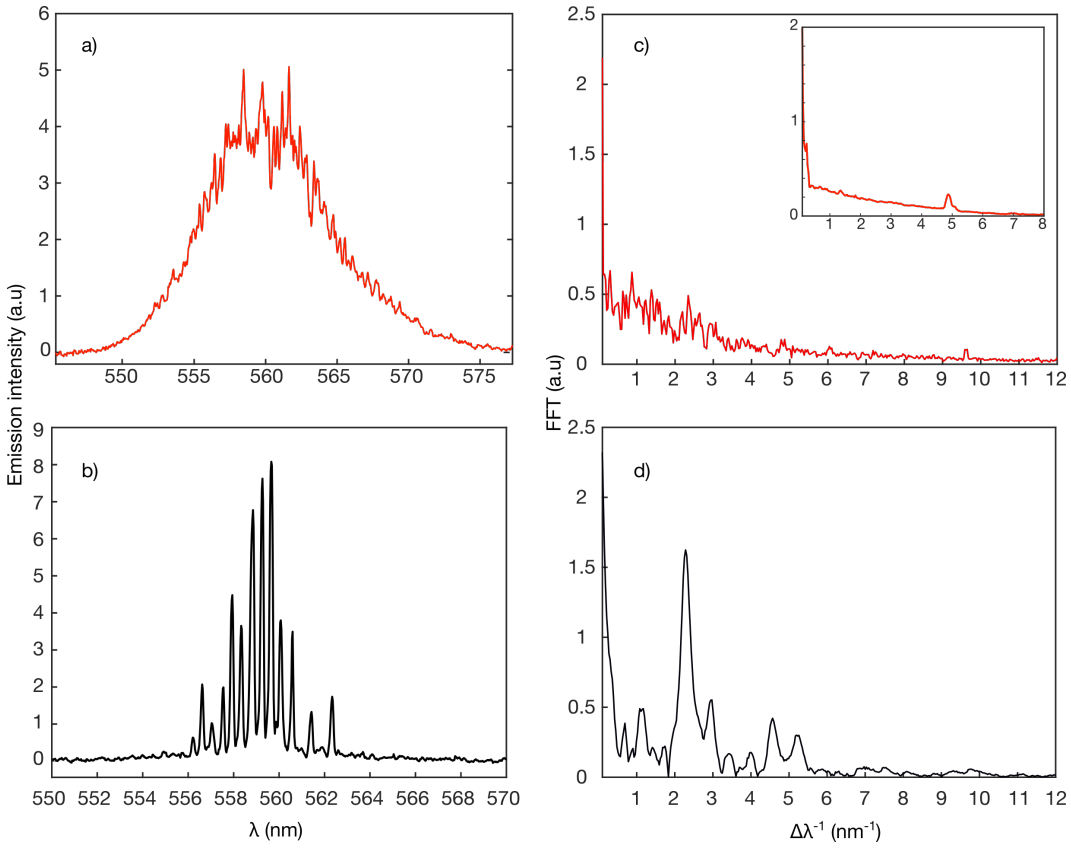

Figure 3.2: a) Typical ASE emission spectrum. b) Example of a periodic emission spectrum of a random laser shot. c) Fourier Transform of ASE emission. The inset is an average of over ~ 300 ASE emission shots. d) Fourier Transform of RL emission shot.

deviation of 20%. The associated cavity length L_c to the measured $\Delta\lambda$, assuming 1.37 as the effective refractive index for the solution, is ~ 300 μm. The ASE emission from the clear dye do not show any evident spectral periodicity, this is probably due to the absence of feedback mechanisms, as verified over a large statistic of shots (Figure 3.2.c). By averaging over 300 ASE emission shots, a small broad peak at 5 nm^{-1} appears in the FT spectrum (inset of Fig. 3.2.c) which is merely caused by the interference of multiple reflections between the two plane-parallel facets of the cuvette wall, corresponding to a path length of 550(30) µm.

Different emission features have been observed by varying the dye concentration. Figure 3.3 reports the average of 30 Fourier Transform of emission spectra, exhibiting prominent and equispaced peaks (as those of of Fig. 3.2.b), for three different dye concentrations of 45mM, 15mM, 5mM and a fixed particles concentration of 10^9 cm^{-3}. By decreasing the dye concentration, the penetration length of the pump increases as well as the gain volume, as it is shown by the lateral images (inset of panels a)-c)) showing ASE and/or fluorescence emissions, since random lasing mainly occurs in the longitudinal direction. Figure 3.4 shows the angular distributions of some sequential random laser shots. In the studied weakly scattering systems the gain volume mainly extends along the pump direction, then also emissions maintain the same directionality. As a result the angular spread of the modes is below 2°.

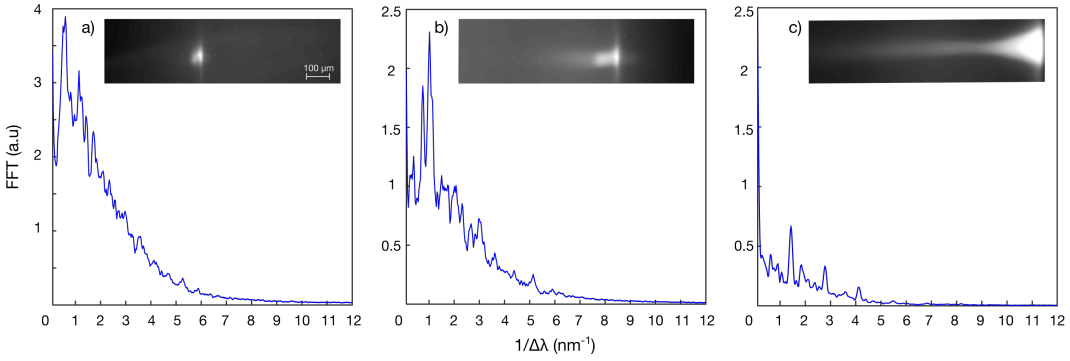

Figure 3.3: a),b),c) Average of the Fourier Transform spectra of 30 periodic RL sample with a dye concentration respectively of 45mM, 15 mM, 5 mM. The insets correspond to the images of emission at ninety degrees with respect to pump axis.

By reducing absorption the cavity enlarges, and the FT peak moves toward

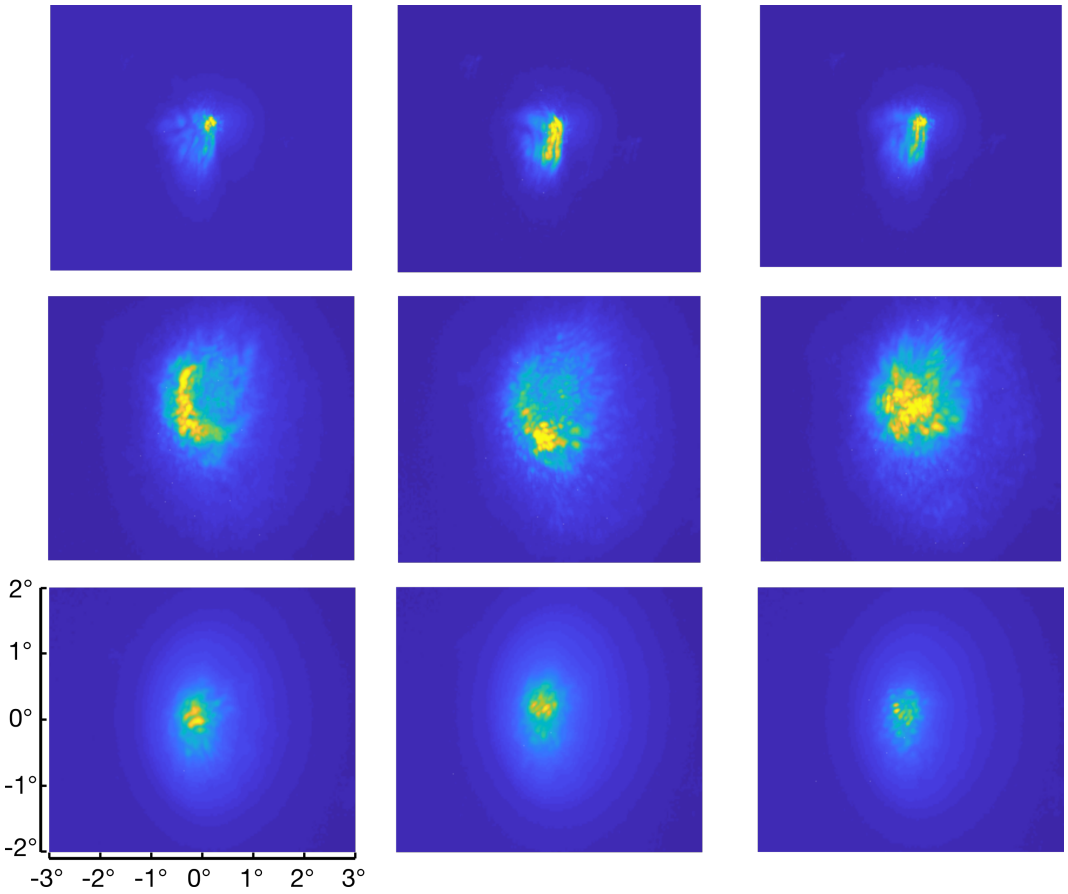

Figure 3.4: Angular emissions of different random laser shots. The images of the angular distribution is obtained by imaging the collimated output of the microscope objective lens. Indeed, since the sample is in the focal plane of the objective, the collimated beam is Fourier Transformed by the objective lens forming an angular-resolved image at its back-focal plane.

higher frequencies ($\frac{1}{\Delta\lambda}$=$2nL/\lambda^2$) consistently with this interpretation.

In the average FT spectra of Figure 3.3, in particular in that of panel c), one can recognize a peak corresponding to the inverse of a mean periodicity in the emission spectrum and other Fourier components with decreasing intensity separated by a multiple of the frequency of the principal peak, usually corresponding to higher harmonics. Additional peaks can also appear not exactly at frequency multiples and they are most probably due to intensity fluctuations of the emission, as will be clarified in the following discussion.

The cavity lengths L_c calculated from the FT peaks of Figure 3.3 are reported in panel a) of Figure 3.5 versus the dye concentration. However, they do not correspond to the penetration lengths of the pump inside the sample as observed by [6]. By considering for example the 5mM sample (Fig. 3.3.c), the estimated mean cavity length is 300 (70) μm from the FT, whereas the penetration length estimated by the fluorescence of the lateral image (inset) is approximately 600 μm. The pump photon flux is of $2{\cdot}10^{28}$ cm^{-2}s^{-1} – assuming a 50 μm of spot radius at the sample interface – which is ∼1000 times larger than the saturation intensity $\sim 2{\cdot}10^{25}$ cm^{-2}s^{-1} (calculated as $1/\sigma_{st}\tau$ with a cross section for stimulated emission $\sigma_{st} \sim 1{\cdot}10^{-16}$ cm^2 and a fluorescence lifetime $\tau \sim 1$ ns). Panel b) of Figure 3.5 for a fixed dye concentration of 5mM shows that L_c it is practically insensitive to variations of the scattering mean free path over more than one order of magnitude (20 μm to 570 μm).

Figure 3.6 shows three subsequent side images and the Fourier transforms of their respective emission spectra. From top to bottom a single cluster, of ∼3 μm, appreciably distinguishable from the image background, is falling through the light beam. When the particle is outside the beam (panel a)) nothing is noticeable in the Fourier Transform spectrum, but when the particle enters in the light beam cone (panel b)), a higher peak near 3.2 nm^{-1} and other smaller ones appear in the FT, becoming more intense and less noisy as the particle gets more illuminated in the centre of the light beam (panel c). In panel c) the major peak in the FT corresponds to a cavity length of 370(30) μm, while the distance between the particle and the cuvette, obtained by the side image, is 360(10) μm. A minor, broader peak at 6.3 nm^{-1} represents the higher harmonic component, while the peak at 5.2 nm^{-1} is ascribed to the cuvette thickness 520(10) μm (compatible with the value of 550(30) μm, due to the fabrication tolerance). As concerns the other peaks in the FT, resonances inside the cluster are excluded, since the first

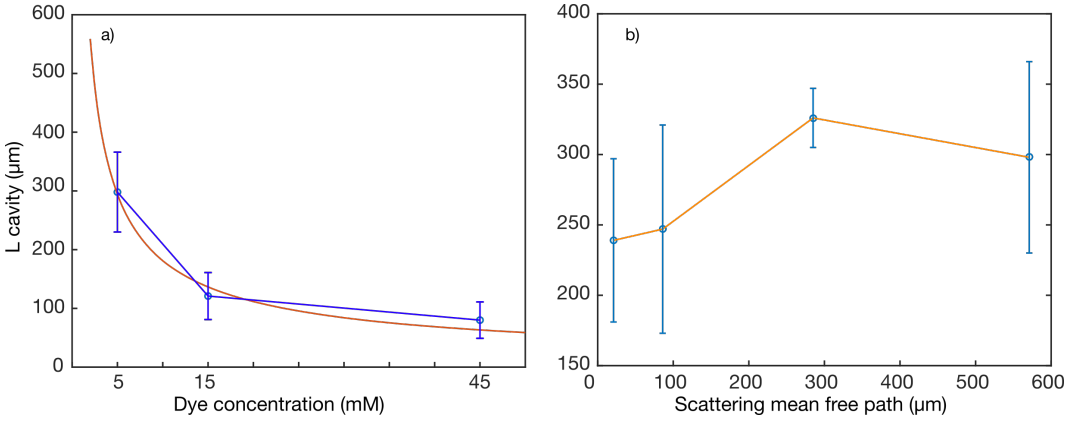

Figure 3.5: The panel a) plot reports the cavity lengths L_c, for three different value from the peak FT. Panel b) shows the cavity length as a function of the scattering mean free path, Lc results substantially independent from this parameter and then from the scatterer concentration.

prominent peak appears around 0.8 nm^{-1}, corresponding to a length of the order of 50 μm. To explain the origin of these secondary peaks, we show in Figure 3.7 the spectra and the relative Fourier Transforms of three sequential emission shots corresponding, analogously to Figure 3.6, to a particle passing through the light beam, where correspondences are particularly evident.

Panel a.I shows the spectrum of a particle that is just entered in the light beam and lasing appears. The Fourier Transform (panel a.II) shows a series of peaks, the first at 0.4 nm^{-1} (blu arrow) followed by other ones with decreasing intensities towards higher frequencies. The one at 1.7 nm^{-1} (black arrow) corresponds to the visible fine periodicity of 0.6 nm in the spectrum on the left panel, which can be directly related to the distance of the particle from the cuvette interface. The peak at 0.4 nm^{-1} and its higher order harmonics (0.8^{-1},1.2 nm^{-1}) are essentially caused by the intensity fluctuations of the lasing modes: it is clear from the left panel, that the two intense peaks distant 2.5 nm induce in the Fourier Transform a more intense peak at 0.4 nm^{-1}. It is therefore sufficient to have just a couple of two more intense peaks in the emission spectrum to create “artificial” peaks in the Fourier Transform spectrum, that are not directly associable to an existent short cavity inside the sample. The same is probably true for the other secondary peaks for which the correspondences are more complex to individuate. Panel b.I shows the emission spectrum when the same particle is fully

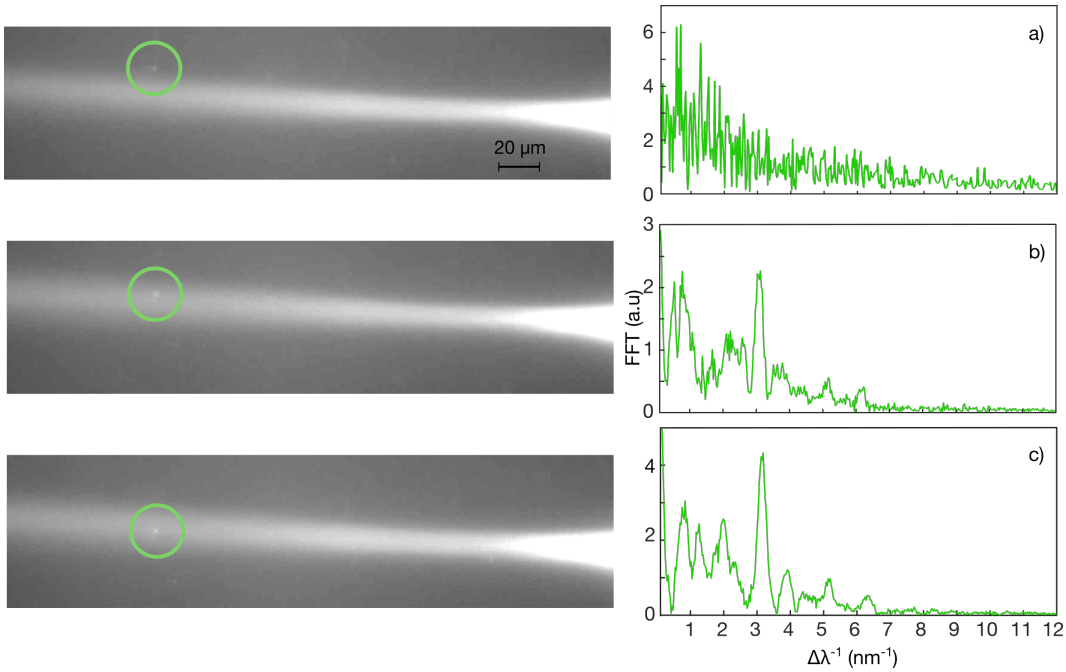

Figure 3.6: From top to bottom, three subsequent images of the liquid and the ASE emissions shots. The green circle evidences a particle moving in the liquid and crossing the light beam. Its distance from the cuvette inner face corresponds to the cavity length extracted from the peak in the Fourier Transform spectra relative to the RL emission at that instant. The peak in the FT corresponds to the inverse of the FSR of the Fabry-Perot like cavity created by the presence of the particle and the cuvette margin. When the particle is perfectly immersed in the light beam the peak in the FT is enhanced, when it is entering or outing in the light beam, the FT peaks goes down.

illuminated by the light beam. Correspondingly, the emission intensity increases by a factor ten, thanks to the enhanced coherent feedback provided by the presence of the scattering particle. The Fourier Transform is dominated by the peak at 1.7 nm^{-1} and the higher harmonic orders 3.5 and 5.3 nm^{-1}, as highlighted in the inset of panel c.II. Eventually, when the particle goes out of the light beam, the spectrum is characterized by an alternation of weakly lasing modes and ASE emission (panel c.I,c.II).

The same experiments have been conducted on several samples, varying both dye and particles concentrations. By pumping slightly above the threshold to observe random lasing, it has been observed that all the times that the emission spectrum becomes periodic a small cluster passes through the light beam, as that reported in Figure 3.6.b. The side images provides a one-to-one correspondence between the cavity length calculated from the emissions and the particle distance from the cuvette front window. Also scattering particles that do not form "big" clusters can be responsible of spectral periodic feature. In some case it is possible to observe periodic spectra without finding cluster in the images, meaning that the particle is too small to be resolved by our imaging system (the resolution of the imaging system allows to clearly distinguish objects with a size greater than 2 µm, to be compared with the average diameter of 400 nm of isolated scattering particles). However the estimated cavity length remains almost the same, considering the same sample, even if the particle is not visible. The particle or the small cluster of particles probably behave as one mirror cavity, while the second mirror is always provided by the cuvette face. This is a small but significant difference from the interpretation given by Wu *et al.* which required the presence of two particles at both the extremities of the light penetration length [6]. In contrast, we have never observed two or more clusters falling down during a sequence of periodic spectra. We have seen that the position of the falling particle is critical to achieve the comb-like spectral emission, which is entirely suppressed as soon as the particle leaves the central part of the pumping volume. For this reason, the estimated probability of having two or more particles fulfilling at the same time these stringent conditions seems negligible for the particle concentration values investigated here and in the work of Wu *et al.*

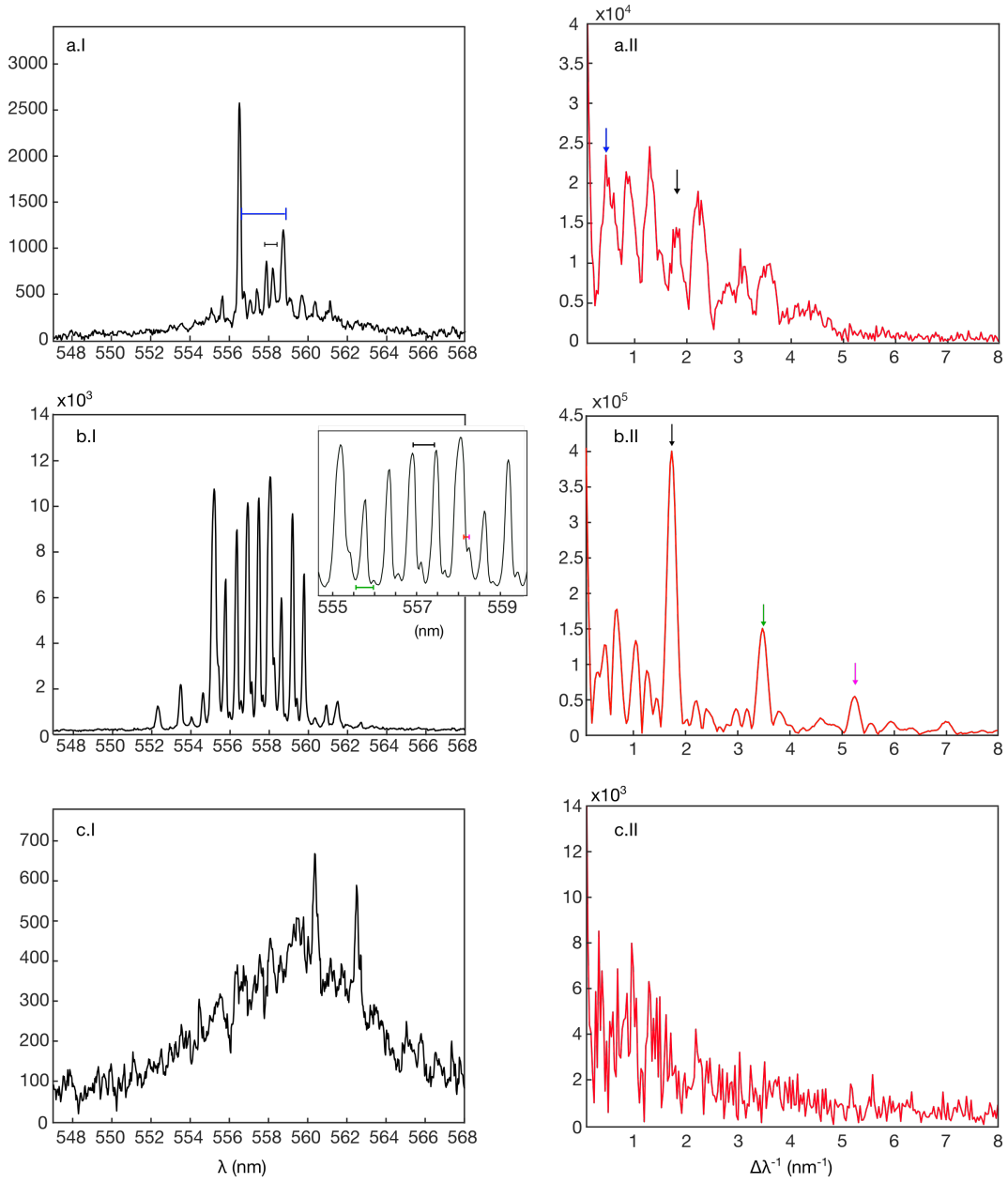

Figure 3.7: Spectra and the relative Fourier Transforms of three sequential emission shots corresponding, analogously to Figure 3.6, where a particle is entering (panel a)), crossing (panel b)), and outing (panel c)) from the light beam.

3.3 Discussion

In the previous section, we have seen how the penetration length of the pump beam estimated from the side images is longer than the effective cavity length that is estimated from the spectral mode spacing (see Figure 3.6). A possible explanation is that the particle or the cluster can build lasing oscillations only if it crosses the light beam up to a maximum distance from the the entrance of the excitation beam which is of the order or greater than the threshold gain length. Then, the cavity extends from the inner face of the cuvette to the position of the particle, like it happens in a regular laser with two reflecting mirrors.

Ito & Tomita in 2004 performed numerical simulations of a random laser in a spherical multiple scattering medium [10]. They studied how the gain volume increase, in random lasing emission, when saturated absorption occurs in the excitation process. For very weak excitation energy the size of the gain volume increases with a one-third power of the excitation energy, until it reaches a critical value where the threshold energy for lasing is surpassed. The size of the gain volume as well as the threshold for lasing depend on dye concentration and transport mean free path. The relation for the energy balance of a random laser system, assuming that the whole excitation photon rate E contributes to pump the active medium and that all the molecules of dye are in the excited state is [10]:

$$E = L_g^3 N \left(\frac{1}{\tau} + c\sigma_{st} s \right) \tag{3.2}$$

Where the first term represents the spontaneous emission process and the second the stimulated emission, N is the dye concentration, τ is the excited state lifetime and s the emitted photon density. The emission light escapes from the gain volume by a diffusion process, then the number of emitted photons has to be equal to that given by the diffusion:

$$L_g^3 N \left(\frac{1}{\tau} + c\sigma_{st} s \right) = \frac{L_g^3 s}{\tau_d} \tag{3.3}$$

with $\tau_d = L_g^2/(l_t c)$, which is the diffusion time employed by light to diffuse outside the gain volume and l_t the transport free mean path. For weak excitation, stimulated emission can be ignored and the gain length reduces to:

$$L_{\mathrm{g}} = \left(\frac{E\tau}{N}\right)^{1/3}, \tag{3.4}$$

which depends with 1/3 power on the excitation rate E. Under strong excitation energy, the size of the gain volume is independent from excitation energy and spontaneous emision can be neglected in equation 3.3 :

$$L_{\mathrm{g}} = \left(\frac{l_{\mathrm{t}}}{N\sigma_{\mathrm{st}}}\right)^{1/2} \tag{3.5}$$

At the lasing threshold condition equations (3.4) and (3.5) can be both equated to the threshold gain length $\mathrm{L_{th}}$:

$$L_{\mathrm{th}} = \left(\frac{l_{\mathrm{t}}}{N\sigma_{\mathrm{st}}}\right)^{1/2} = \left(\frac{3\sigma_{\mathrm{a}}}{\sigma_{\mathrm{st}}}\right)^{1/2} L_{\mathrm{a}} \tag{3.6}$$

Where σ_{a} is the absorption cross-section, l_{a} the absorption length and L_{a}=$(l_{\mathrm{a}} l_{\mathrm{t}}/3)^{\frac{1}{2}}$ the diffusive absorption length. In Figure 3.8 we report the diffusive absorption length L_{a} we estimated from lateral imaging, versus the mean cavity length for the three dye concentrations relative to the average of the FTs of random laser emission spectra (Figure 3.3). The trend for the cavity length is in good accordance with (3.6). The relation between L_{a} and L_{c} seems to validate the hypothesis that L_{th} and L_{c} are strictly connected, and it also explains why the other particles within the light beam, if any, do not contribute to create other cavities with shorter lengths. Indeed, particles passing in the centre of the beam do not reach the threshold length to build up lasing oscillation through backward scattering, while those that are far beyond that length, where the pump is weaker, incur in much stronger reabsorption effects. Indeed, the average values for cavity lengths show only a rather limited $\sim$ 20% relative standard deviation, which for the three different dye concentrations correspond to the threshold lengths needed to achieve lasing mechanisms.

In conclusion we studied the emission spectra of random laser shots, obtained from a liquid, weakly scattering sample of nanoparticle and dye at various concentrations, and examine the mechanism responsible for the observation of equidistant lasing peaks. The synchronous acquisition of the lateral images of the liquid and the emission spectra allowed to relate the spectral periodicity of

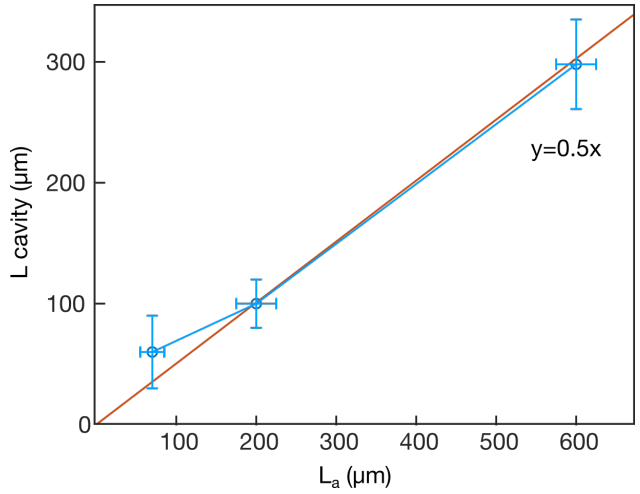

Figure 3.8: Diffusive absorption length L_a estimated from lateral imaging, versus the mean cavity lengths L_c for the three dye concentration. These are estimated from the average of the FTs of random laser emission spectra.

the emission shots to the configuration of the scattering suspension at those instants. By examining many different emission shots, we found an exact correspondence between the spectral periodicity and the presence of a single small cluster of particles falling across the light beam, visible in the lateral images. The retrieved cavity lengths are in excellent agreement with the distances between the cluster and the cuvette face measured from the images. Moreover by repeating the same characterization for three different dye concentrations we observe that the cavity lengths do not show any significant dependence from the scattering strength and are mostly determined by the dye concentration alone. Under high gain saturation conditions, following Ito & Tomita we find a link between the absorption length and the cavity length. We estimate from experimental measurements that the cavity length corresponds, within certain margins, to the threshold length required for lasing inside the medium. It is sufficient that a single cluster or a particle moving randomly through the suspension, passes through the beam at a distance from the cuvette wall equal to the threshold length to give rise to the regular comb-like emission of narrow lasing peaks. Bigger clusters are typically associated to higher feedback enhancement, which explains why even a single scatterer can enhances periodicity, being the second

mirror provided by the cuvette interface.

References

1. Frolov, S., Shkunov, M., Fujii, A., Yoshino, K. & Vardeny, Z. Lasing and stimulated emission in /spl pi/-conjugated polymers. *IEEE Journal of Quantum Electronics* **36,** 2–11 (Jan. 2000).
2. Frolov, S. V., Vardeny, Z. V., Yoshino, K., Zakhidov, A. & Baughman, R. H. Stimulated emission in high-gain organic media. *Physical Review B* **59,** 5284–5287 (Feb. 1999).
3. Polson, R. C. & Vardeny, Z. V. Spatially mapping random lasing cavities. *Optics Letters* **35,** 2801 (Aug. 2010).
4. Polson, R. C., Raikh, M. E. & Vardeny, Z. Universality in unintentional laser resonators in -conjugated polymer films. *Comptes Rendus Physique* **3,** 509–521 (Jan. 2002).
5. Mujumdar, S., Ricci, M., Torre, R. & Wiersma, D. S. Amplified extended modes in random lasers. *Physical Review Letters* **93** (2004).
6. Wu, X. *et al.* Random lasing in weakly scattering systems. *Physical Review A* **74,** 053812 (Nov. 2006).
7. Hardy, A. Amplified Spontaneous Emission and Signal Amplification in Dye-Laser Systems. *IEEE Journal of Quantum Electronics* **11** (1975).
8. Haag, G., Munz, M. & Marowsky, G. Amplified Spontaneous Emission (ASE) in Laser Oscillators and Amplifiers. *IEEE Journal of Quantum Electronics* **19,** 1149–1160 (1983).
9. Abraham, N. & Rockower, E. Amplified-spontaneous-emission intensity fluctuations. *Phys. Rev. A* **24** (Nov. 1981).
10. Ito, T. & Tomita, M. Analysis of gain volume in random laser in a spherical multiple scattering medium. *Optical Review* **11,** 7–11 (2004).

Chapter 4

Optical super-resolution

4.1 Super-resolution techniques for imaging and spectroscopy

The general concept of super-resolution relates to the methods used to recreate a higher quality signal using sets of low-resolution measurements. In recent years various optical techniques able to achieve a resolution beyond the diffraction limit or more simply the instrumental resolution were proposed, ranging from imaging techniques for super-resolution microscopy to reconstruction algorithms enhancing the resolution of a detected interferogram.

Super-resolution microscopy In *near-field scanning optical microscopy* (SNOM) the excitation laser light is focused through an aperture with a diameter smaller than the excitation wavelength, resulting in an evanescent field on the far side of the aperture. When the sample is scanned at a small distance ($< \lambda/50$) below the aperture, the optical resolution of transmitted or reflected light is limited only by the diameter of the aperture. This allows to generate images that resolve details of nano-scaled samples [1]. More recently optical masks have also been designed to remove the need of the evanescent field by achieving a sub-wavelength focus at a distance beyond their typical reach. This means that the object to be imaged does not need to be in the immediate proximity of the superlens. This device can be used to perform super-resolution imaging for example on a living cell, which would be otherwise impossible to investigate with a near-field device [2]. In the

far-field, many fluorescence light microscopy techniques have been developed to improve the study of biological specimens. Using these techniques, novel mechanisms in nerve growth and new properties of synapses have been revealed [3]. Some of these techniques, whose importance was emphasized by the 2014 Nobel Prize for chemistry, are based on the clever concept of sparse spatial sampling, which allows to map an image, point by point, at high resolution. The *Stimulated emission depletion microscopy* (STED) is a deterministic technique that exploits the non-linear response of emitting fluorophores. An exciting beam is focused by an objective lens on the fluorophores. According to diffraction limit, the intensity distribution in the focal plane represents the point-spread-function (PSF). To increase resolution, the extension of the excitation area is reduced by inhibiting the fluorescence in the outer regions. This mechanism is achieved with an additional light beam, the STED beam, that induces stimulated emission at the borders. This allows to locally deplete the population of the excited state, so that only the innermost region contributes to the fluorescence signal [4].

Conversely, stochastic techniques as *Photo-activated localization microscopy* (PALM) and *Stochastic optical reconstruction microscopy* (STORM) use mathematical models to reconstruct a sub-diffraction image from many sets of diffraction limited images. In STORM, photo-switchable molecules as the cyanine dye Cy5 are probed continuously by a low-intensity red laser beam. An additional red pulse converts the molecules to a non-fluorescent "dark" state, while a green pulse can bring them back to the fluorescent state. A secondary chromophore, Cy3, facilitates the switching of Cy5 to a light state[5]. In PALM, numerous sparse subsets of fluorescent protein molecules are activated by a light beam, localized and then bleached. This process is repeated for many cycles, depending on the spatial distribution of the molecules, until the population of inactivated and unbleached molecules is depleted [6, 7]. Then for both techniques, only a sparse and optically resolvable subset of point-like sources is activated to a fluorescent state, allowing to determine their position by fitting the centroids of the blurred disk generated by each point source. Following the repeated identification of such sources over a large amount of frames, a complete, sub-diffraction image is obtained.

Compressed-sensing and reconstruction algorithms A separate discussion regards the techniques based on compressed sensing (CS) algorithm, which have

been applied to the reconstruction of both images and spectral data. For example, in conventional far-field imaging, sub-wavelength information is lost due to the decay of evanescent waves. The problem is equivalent to that of recovering an original signal after been filtered from a low-pass filter. In practice this is possible if we have the a priori knowledge that the signal is sparse [8]. For a signal to be sparse means that there exists a certain mathematical basis where its representation comprises a very small number of elements with non-zero projection in that basis. An essential result of CS is that it is enough to choose a measurement basis that is uncorrelated with the signal basis. This important theorem indeed ensures that if the signal is sparse in one of the bases, it will give rise to a dense representation in the other. An example of maximally uncorrelated bases are the spatial and the Fourier domains. One of the most common algorithms to recover the signal in practice is the basis-pursuit method, it involves the minimization of an L_1 norm, and can be implemented quickly and efficiently [9]. Being $\boldsymbol{b}$ the linear measurement of the original signal $\boldsymbol{x}$: $\boldsymbol{b} = \boldsymbol{A}\boldsymbol{x}$, where the matrix $\boldsymbol{A}$ is a known measurement function. If $\boldsymbol{x}$ is sparse, it can be exactly recovered by minimizing its L_1 norm

$$\text{minimize } ||\boldsymbol{x}||_{L_1} \text{ subject to } \boldsymbol{b} = \boldsymbol{A}\boldsymbol{x}$$

even when $\boldsymbol{x}$ has far fewer elements than $\boldsymbol{b}$. Both STORM and PALM are based on the imaging of sparsely distributed single-molecules. In these techniques only a portion of the sparsely distributed molecules is imaged and localized in each raw image, requiring thousands of raw images. CS can for example increase the maximum density of fluorescent molecules in a raw image, even if these fluorophores are not distributed so sparsely and their images overlap with one another [10, 11]. Moreover sparsity provides an effective tool for overcoming the fundamental resolution limit of spectroscopic devices. Sidorenko *et al.* use the sparsity-based concepts of CS to demonstrate the recovery of spectral features at a resolution exceeding the fundamental resolution limit of a FTIR spectrometer [12], while Katz *et al.* can achieve the resolution of a N-point Fourier spectrum from much less than N time-domain measurements using a compressive-sensing reconstruction algorithm [13].

Among the existing reconstruction methods to increase the resolution of a frequency spectrum there is the maximum entropy method (MEM) [14]. The idea is to choose the spectrum which corresponds to the most random time series

whose autocorrelation function agrees with a set of known values. The method derives its name from the same concept of maximum entropy used in information theory. The algorithm operates a reconstruction of the frequency spectrum applied to Fourier transform spectroscopy data (interferogram) producing a spectral estimation with enhanced resolution [15].

Deconvolution in spectroscopy In spectroscopy, the overlapping of spectral components results in line-broadening when the instrumental resolution is too low. This typically happens in Fourier-Transform spectrometers where the interferogram is limited by the maximum delay time, or in a dispersion spectrometer where the spectral response to a delta-function translates to a line of finite width. The artificial resolution improvement that results in a partial separation of spectral data and decomposition of a composite spectrum into individual pure-component spectra is defined as deconvolution. Deconvolution can upgrade the resolution of a spectroscopic measurement up to 2-3 times. From the theoretical point of view, deconvolution is generally considered as an inverse problem, which is commonly encountered in practical applications. The problem posed in spectroscopic terms is that of retrieving the true spectrum from that measured by using the instrumental response function. A deconvolution method widely used is Fourier self-deconvolution (FSD) which was developed on the basis of Fourier transform spectroscopy [16].

$$S(x) = \int_{-\infty}^{\infty} K(x - x')R(x')\,dx' \tag{4.1}$$

where S is the measured spectrum, K the instrumental response function and R the true spectrum. By the knowledge of the instrumental response function and the the measured spectrum, we can retrieve the true spectrum. Stationary convolution from the spatial to the frequency domain is commonly implemented using integral Fourier transform :

$$\tilde{S}(\omega) = \tilde{K}(\omega)\tilde{R}(\omega) \tag{4.2}$$

Since for $\omega \to \infty\ \tilde{K}^{-1}(\omega) \to 0$, the deconvoluted spectrum is evaluated within a regularization window (i.e a filter) W that at infinity must decay more rapidly than the response function. Then:

$$R(x) = \frac{1}{2\pi}\int_{-\infty}^{\infty} W(\omega)\tilde{K}^{-1}(\omega)\tilde{S}(\omega)e^{jx\omega}\,d\omega \tag{4.3}$$

It is evident from eq. 4.3 that deconvolution is the solution of an inverse ill-posed problem, where disturbances of the instrumental function and of the measured spectrum as well as truncation effects may cause computational errors of $R(x)$. Common mathematical methods can be used to obtain a more stable solution, and are usually based on a priori assumptions concerning the mathematical representation of the instrumental function and/or its properties. Prior knowledge of the response function, however, poses another problem. The vast majority of deconvolution algorithms are still based on that knowledge and their performance degrades quickly for incorrectly presumed instrumental response functions. To date, no method is known for the exact determination of the response function of an instrument. To circumvent this issue, blind deconvolution has also been proposed as an iterative algorithm that allows to improve the estimations of both the ideal spectrum or image and the effective response function of the instrument [17, 18].

4.2 A new concept of spectral super-resolution

In this section we describe the basic concepts and the idea underlying a novel technique to achieve super-resolved spectral reconstruction. Following an introductory part, we discuss first a set of numerical calculations that we have performed to test its validity limits, while Chapter 5 is entirely dedicated to the first experimental demonstration of its applicability.

In this work, the concept of sparse sampling in the frequency domain is used to achieve a super-resolved spectral characterization of an unknown sample, similarly to the case of super-resolution microscopy with spatial sparse sampling. In this case, the resolution limit is posed by the spectral resolution of a dispersive spectrometer which is not sufficient to characterize a sample with spectral features that are finer than the nominal resolution of the measuring instrument.

The resolution of a spectrometer is defined using the Rayleigh criterion [19], i.e. its ability to identify two adjacent spectral lines. This is strictly connected with the "instrumental line profile", $I(\lambda)$, corresponding to the spectral line measured by a detector at the output slit if a "monochromatic field" is focused at the spectrometer entrance slit. The FWHM of $I(\lambda)$ defines the spectrometer resolution. This implies that any spectrum $S(\lambda)$, analyzed by the spectrometer, is the

result of the convolution of the real spectrum $S_0(\lambda)$ with the instrumental line profile $I(\lambda)$: $S(\lambda) = S_0(\lambda) * I(\lambda)$ (eq. 4.1).

The shape of $I(\lambda)$ depends both on the properties of the spectrometer and the detector; if the latter is realized by an array, the spatial density and arrangement of the pixels concur to determine the instrumental resolution. As a rule of thumb, if the monochromatic line is not resolved by at least three pixels, then the resolution of the measurement is clearly limited by the detector rather than the monochromator. In the following, unless otherwise specified, we will always assume that the instrumental resolution is not limited by the properties of the detector. This corresponds to the most relevant situation in many cases. If the light source has an emission characterized by peaks with a natural widths that is narrower than the instrumental resolution, then the FWHM of the recorded peaks coincides with that of the instrumental profile. Even if the spectral features to be determined are below the spectral resolution of the apparatus, we are able, within certain validity limits described in the following, to obtain a super-resolved characterization of the transfer function of a sample.

4.2.1 Simulation of a spectral-super resolution experiment

In the following, we describe an alternative strategy to reconstruct the transmission curve of an unknown sample without using white light illumination and therefore avoiding the need to resort to deconvolution. Our approach leverages instead random sparse sampling of the unknown curve to progressively refine its reconstruction, similarly to what stochastic microscopy applications have demonstrated for imaging purposes. The main novelty of the method, and what makes it unique with respect to previous stochastic reconstruction methods, is to employ the random laser as narrow line emitting source which is inherently characterized by a stochastic spectral response. We retrieve the target transmission function by performing a sparse frequency sampling exploiting the intrinsic properties of random laser in the chaotic regime. As described in Chapter 2, when a random laser is working in a pulsed regime, and above threshold, it exhibits a chaotic emission spectrum with a set of narrow lasing modes fluctuating in frequency and amplitude at each shot of the pump laser. To this purpose the resulting series of sparse, sharp and uncorrelated laser peaks allows to probe the spectral response of a sample and reconstruct the transmission spectrum with

enhanced resolution, despite using a low resolution spectrometer and without a precise knowledge of the instrumental response. In this section we illustrate and demonstrate the idea providing theoretical insights on the parameter space of operation and the results obtained with this method are compared with that obtained from a standard deconvolution process. Let us consider as a starting sample a low-finesse Fabry-Perot (FP) filter characterized by a free spectral range (FSR) well below the spectral resolution of a measuring apparatus (FWHM= 4.9·FSR). The outline of the setup is shown in Fig.4.1, which was also used as a guide to set up the numerical simulations. This outline also serves to illustrate the idea more in detail. Two types of light sources have been considered: a random laser (purple in the figure) and a regular lamp for comparison (yellow in the figure). The transmission of the etalon is measured versus frequency, using a low resolution spectrometer (indicated in green, together with its (broad) spectral response function). In the yellow graph (panel b) the optical response is shown when the sample is illuminated with an ideal Gaussian-shaped broadband illumination source. Due to convolution of the transmission spectrum of the sample with the (broad) instrumental response function of the spectrometer, the Fabry-Perot fringes disappear almost completely. From a mathematical point of view, by knowing I(λ) exactly for an ideal delta-like source, it would still be possible to recover the original signal using a deconvolution operation. However, this is unfeasible in practice due to the finite noise level of a real measurement, and it is in fact already challenging even in this simulated case due to numerical instability of deconvolution, which is highly susceptible to the finite precision of computed functions [17, 20].

Numerical simulations have been performed on large sets of computer generated spectra with a random laser illumination source. In Fig. 4.1.d, examples of the numerically simulated transmission spectra have been plotted. These shots represent the random laser operating in the chaotic regime, where only few modes actually reach threshold leading to the typical random laser emission spectrum that consists of few narrow 'spikes', well-separated from each other. In the chaotic regime of operation, the emission spectrum of each random laser pulse is completely uncorrelated from the previous pulse. These are precisely the properties that make the random laser an ideal source for sparse sampling in the frequency domain. In each transmission curve, one can identify isolated broadened peaks arising from the convolution of the narrow mode (fuchsia curves) with the instru-

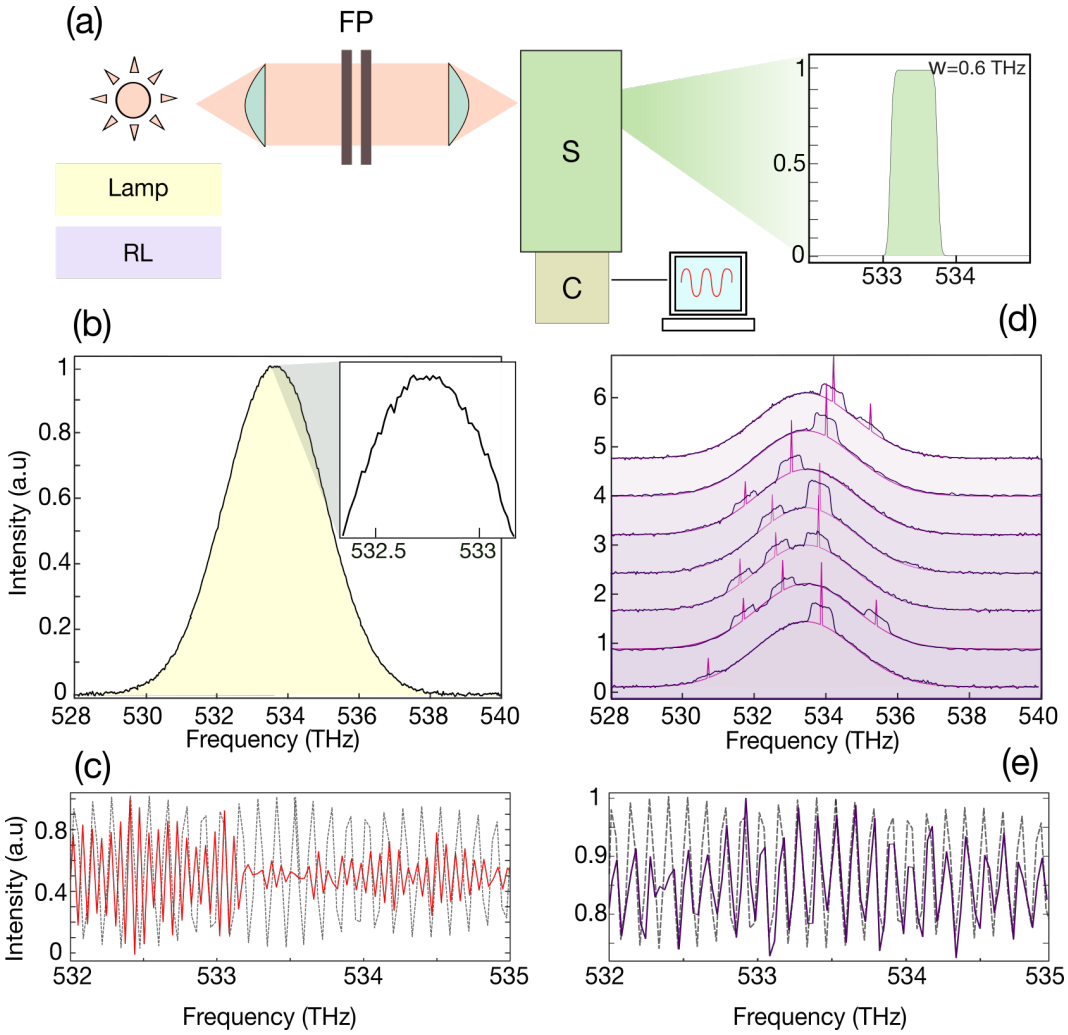

Figure 4.1: a) Scheme of the setup described by the simulations: a light source (either a broadband source or a random laser) is used to measure the transmission function of a Fabry-Perot filter (FP), through a spectrometer (S) with a large point spread function (inset) and a linear camera (C). The assumed spectral dispersion is 36 GHz/pixel, reproducing that of a standard diffraction grating (1200 l/mm) and a commercial linear camera (1248 pixel, 14 μm pixel size). The numerical transmission function of the low finesse FP approximates a sinusoid with FSR of 125 GHz. b) Average of 10^4 numerical broadband spectra modulated by the FP. Because of convolution effect the original contrast is attenuated and almost hidden even by very low noise fluctuation. c) Deconvoluted response (red) obtained by deconvolving spectrum b) from point spread function (inset of panel (a)). Numerical FP response function (dashed grey) as measured by the camera with a spectral resolution of FWHM=4.9·FSR. The deconvolution method fails in retrieving the original response. d) Example of many single shot random laser emission (purple) obtained with the same low spectral resolution setup of (b). In violet is evidenced the intrinsic narrow nature of RL modes, which were pixel-limited in the case of very high resolution spectrometer. e) FP transmission function reconstructed with the method of the peak analysis, performed on a set of 10^4 single shot RL spectra. In the average the original FP contrast is restored as well as the FSR. The fluctuation in the peak transmission is mainly due to the lack of statistics and an unoptimal peak normalization.

mental response function of the spectrometer (inset of panel a)). Despite this peak broadening, it is still possible to identify their center frequency with high precision since there are typically only few prominent peaks for each emission spectrum. Each of the selected peaks provides one data point in the reconstruction of the target spectrum. By recording peak amplitudes and frequencies for the most prominent peaks through a series of chaotic spectra (in the order of a few thousand) and by plotting their amplitudes as a function of frequency, the original transmission function is eventually retrieved with a spectral resolution that exceeds that of the instrument. The reconstructed spectrum is shown in the bottom panel of Fig. 4.1 as obtained using a total of 10^4 single shot RL spectra. For comparison, we also show the result for a broadband source like a regular lamp, using the same parameters. While nearly all information is lost using the broadband source, random laser illumination allows to reconstruct the target spectrum with very good precision. Regular deconvolution is very sensitive to small noise fluctuations – which are amplified in the reconstructed spectrum. The statistical reconstruction using a random laser is much more stable and successfully retrieves the original FP contrast and spectral pattern – especially in the central region where the RL statistics is larger. We have performed a broad range of similar simulations and found that random laser based super-resolved spectral reconstruction can be applied nearly arbitrarily, for a wide range of apparatus response functions and target transmission spectra. In the following section the parameters for spectral reconstruction are discussed more in detail.

4.2.2 Statistics and noise levels for spectral reconstruction

To understand the validity limits that apply to this super-resolved spectral reconstruction, we test the method for many possible experimental configuration, varying the statistics of the random laser spectra and the amplitude of noise fluctuations. The MATLAB codes used to reconstruct the transmission function of the FP filter presented in the previous section are reported for completeness in Appendix 4.3. Figure 4.2 reports the results of the reconstruction algorithm when the FWHM=4.9·FSR, fixing the number of spectra to $1{\cdot}10^4$ and varying the noise amplitudes. The left panel reports the reconstructed FP transmission spectra while the right panel shows the corresponding FT curves, from where we can see that the target spectral feature is lost above a noise level of 20% for a statistical

ensemble of spectra of that size.

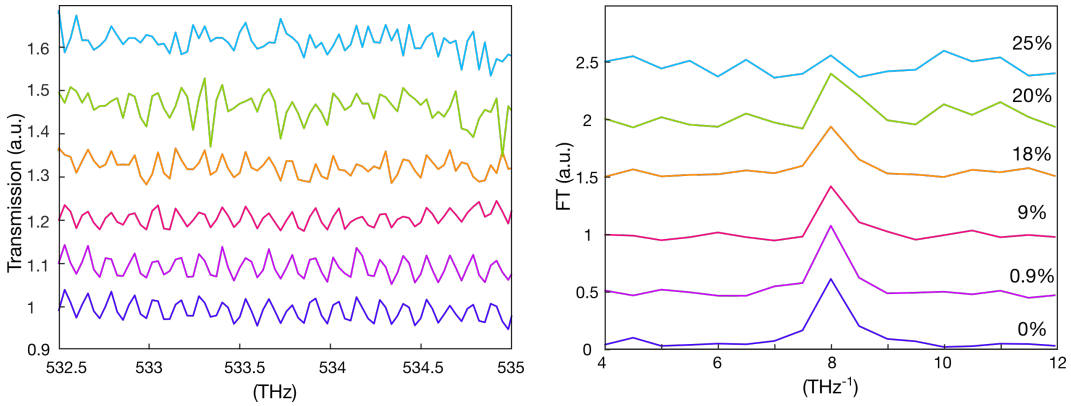

Figure 4.2: *Left)* Reconstructed transmission function resulting from selection of prominent random laser peaks. For each noise amplitude, the numerical random laser spectra are 10^4 . *Right)* Reconstructed FT spectra of the FP transmission function reconstructed numerically through the algorithm. In both panels, curves have been shifted vertically for better clarity.

Figure 4.3 shows the reconstructed curves for a noise level of 1%, when the number of spectra passes from 1000 to 40000. On the right panel, one can see in the Fourier domain how the contrast of target spectral feature with respect to nearby reciprocal frequencies increases when a larger statistics is considered.

We performed a numerical study of how the signal-to-noise ratio of the recovered transmission function varies as a function of the number of spectra. Figure 4.4 describes the trend for the signal to noise ratio (SNR) calculated from the FTs of the reconstructed functions (Figure 4.3), when the number N of collected spectra is increased from 500 to 40.000. The increase of collected spectra is associable to a Poissonian distribution where the accuracy of the reconstruction is found to scale as $\sqrt{(N)}$.

Further simulations with different shapes for the instrumental response (from Rect to Gaussian) and transfer functions (see Figure 4.5) shows that this method can in principle work with functions of different shapes and with any form of spectral responses, as long as the sampling is provided by the detector is enough to resolve the response function with a sufficient amount of pixels. This method is shown to work even when both the resolution is very low and when, under certain limits, the measurement is deteriorated by noise fluctuations. The statistic of the random laser peaks has also been varied from Gaussian to Lévy and

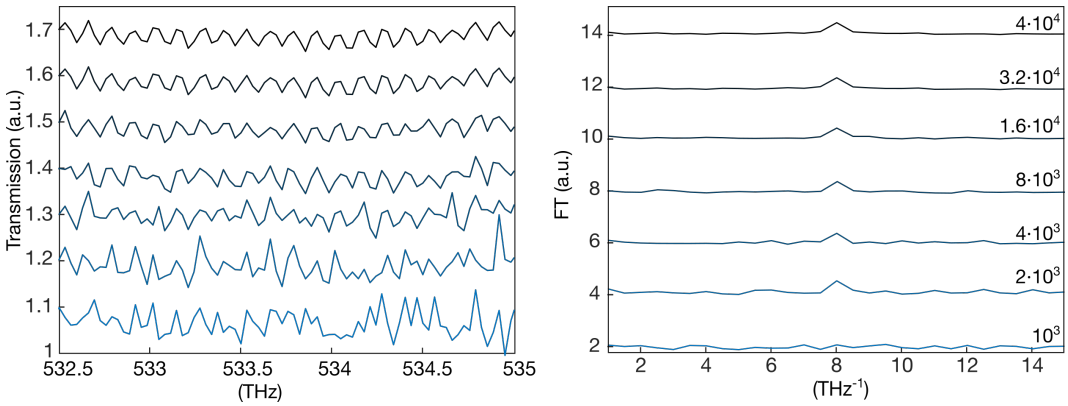

Figure 4.3: *Left)* FP reconstructed curves, for noise fluctuations of 1%, and increased number of spectra from bottom to top. *Right)* FT spectra of the curves in the left panel, showing the signal to noise ratio of the reconstructed curves.

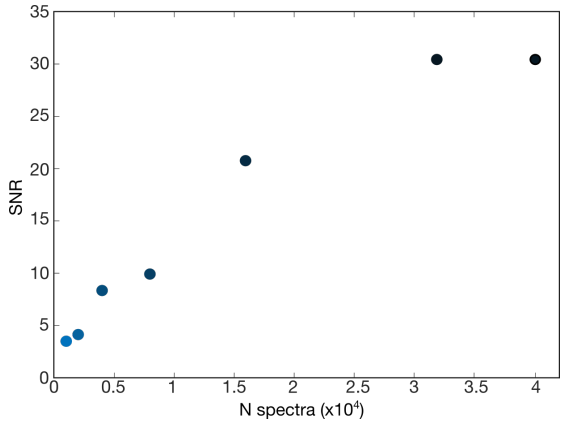

Figure 4.4: The signal to noise ratio of the reconstructed FP transmission function grows sub-linearly with increasing the number of spectra, that is, the number of peaks collected.

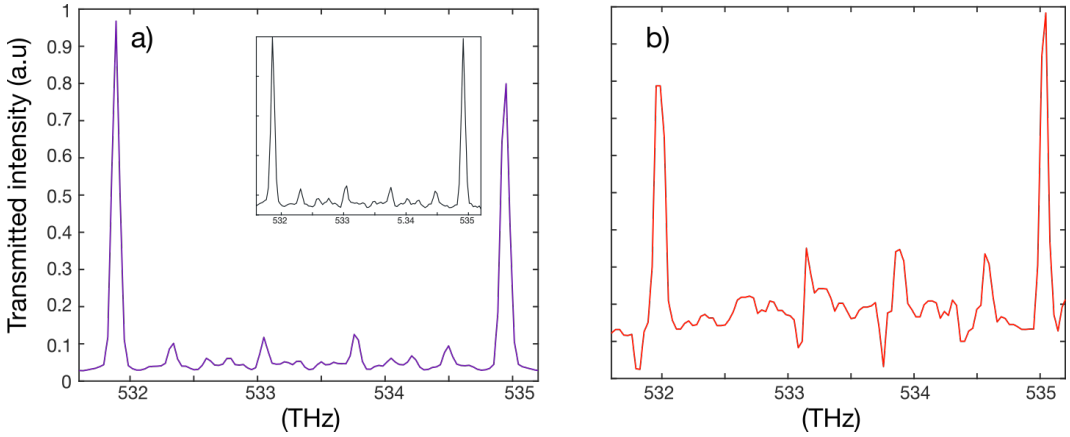

Figure 4.5: a) Numerically reconstructed transfer function presenting a complex structure of spectral features. The transmission function selected is shaping the FT of a multilayer Fibonacci structure (inset). The spectral response and the random laser spectra are the same as reported in Figure 4.1. The acquisition noise is posed to zero. b) Deconvolution does not recover correctly the transfer function even when the noise is absent.

in all these cases similar results were obtained. These results provide a comprehensive stress-test for the validity of the method over a broad range of conditions and in particular give a rough estimate of the required statistics of random laser shots to obtain an experimental evidence of a super-resolved reconstruction. The following chapter contains a full description of the experimental realization of the super-resolution experiment, starting from the sample realization and its spectral characteristics, then describing the optical setup used to reconstruct the transmission features of a Fabry-Perot filter with FSR higher than the spectrometer spectral response.

4.3 Appendix

In this section we report the MATLAB codes used for the realization of the numerical experiment showing the super-resolved spectral reconstruction of the Fabry-Perot filter using the random laser. The algorithm can be divided in three main sections. In the first part the we define the Fabry-Perot transmission function, the fluorescence band and generate a number N of random laser spectra. The spectra generated are the result of the transmission through the FP filter and the dispersion from the spectrometer with spectral resolution resolution equal to G.

```
%%%%frequency axis definition for super-sampled spectra%%%%
c0=2.99792458e8; %m/s = nm*GHz
step=0.05;
z=[1:step:400];
z0=floor(z(end)/2);
lambda0=562; %nm
lambda=lambda0-(0.034)*(-z+z0);
nu_1=c0./lambda; %GHz
[r1,r1]=min(abs(560.5-lambda));
[r2,r2]=min(abs(564-lambda));

%%%%Fabry-Perot filter%%%%
FSR=125; %GHz
A=0.135;
fabry= A+0.018*sin(2*pi*nu_1/FSR);

%%%Gain Medium Curve %%%
 F=100;
flu=exp(-4*log(2)*(z-z0).^2/F^2);

%%%% Generation of N random spectra with a spectral resolution of FWHM=G (in pixel)
N=[1000 4000 10000];
G=[4 20];
for l=1:length(N);
for k=1:length(G);

    x=zeros(length(nu_1),N(l));
    s=zeros(length(nu_1),N(l));
```

```
    e=zeros(length(nu_1),N(l));
    n=zeros(length(nu_1),N(l));

%%%   spectral response  function of the spectrometer (Rect) %%%
  g1=z*0;g1(floor(length(nu_1)/2)-floor(G(k)/2/step): ...
  floor(length(nu_1)/2)+floor(G(k)/2/step))=1;
  c=exp(-4*log(2)*(z-z0).^2/2^2);
  g2=conv(c,g1,'same')*step;
  g=g2/sum(g2*step);


%%%generation of Random Laser Spectra transmitted by the Fabry-Perot filer %%%
 peak_number=3;
 noise=4e-5;

 for j=1:N(l);
   r=abs(floor(random('norm',length(z)/2,F/step,[peak_number,1])));
   ss=union(find(r>length(z)),find(r==0));
   r(ss)=[];
   a=random('Uniform',1-0.5,1+0.5,[length(r),1]);
   rn=randi([1 length(z)],length(z),1);
   an=1e-9+random('norm',0,noise,[1,length(z)]);
   n(rn,j)=an;
   x(r,j)=a;
   x(:,j)=(x(:,j).*flu'+0.01*flu').*fabry';
   s(:,j)=conv(g,x(:,j),'same')*step;
   e(:,j)=s(:,j)+n(:,j);

 end
```

There is an optimal number of peaks that should appear on the gain medium curve, to avoid super-position effects on a curve that is ~4 THz wide, This limit can be qualitatively determined to be around 7. A lower limit does not exist, in theory a single random peak is analogous to a (stochastic) tunable laser.

```
 %%%% resampled spectra to simulate acquisition from a linear camera
%%%%
 px=[1:1:400];
 px0=floor(px(end)/2);
 lambda1=lambda0-(0.034)*(-px+px0); %nm
 nu=c0./lambda1; %GHz
```

```
 f=(length(nu))/((nu(1)-nu(end)));

 e_1=interp1(z,e,px);
 fabry_1=interp1(z,fabry,px);
 flu_1=interp1(z,flu,px);
 g_1=interp1(z,g,px);

 [e1,nu1]=resample(e_1,nu,f);
 [fabry1,nuf1]=resample(fabry_1,nu,f);
 [flu1,~]=resample(flu_1,nu,f);
 [strum,~]=resample(g_1,nu,f);

A1=mean(e1,2);
A1=flipud(A1);
e1=flipud(e1);
fabry1=flipud(fabry1);
```

The N spectra at the output of the spectrometer are resampled as they where acquired by a commercial camera with a limited number of pixels.

Below it is shown the routine for the selection of the random laser peaks. The FWHM of a single RL mode is fixed by the spectral response function of the spectrometer, and depends on its resolution. The peak line-shape is the result of the convolution of the narrow lasing mode with the spectral response of the spectrometer. If two fluctuating modes are closer than the spectral resolution limit, they are unresolved and result in a slightly broader peak, precluding a correct retrieval of the exact peak positions. For this reason a control over the peak distance in the same spectrum is needed to reject modes which are closer than G. The collection of all peak frequencies and amplitudes is stored in a matrix. By plotting this matrix we obtain a clouds of points, where to each frequency positions corresponds multiple peak amplitudes. To obtain the transmission function of the sample, at each frequency bin, determined by pixel width, the average of the peak amplitude is calculated. This operation is necessary in order to compensate for intensity fluctuations of random laser peaks and acquisition noise.

```
%%%routine for peak selection %%%%
sub_nu=[];
sub_nu2=[];
e_sub_nu=[];
```

```
for i = 1:size(e1,2)
y0=smooth(e1(:,i)-A1,5);
y1=gradient(y0);
yout1=gradient(smooth(y1,5));

[~, locs,~] = findpeaks(yout1,'MinPeakHeight',0.6e-5);
     i
    if mod(length(locs),2)==0
       for ii = 1:length(locs)/2;
       if locs(2*ii)-locs((2*ii)-1)<1.1*G(k) && ...
       locs(2*ii)-locs((2*ii)-1)>0.9*G(k)

       sub_nu2= nu1(-1+floor((locs(2*ii)+locs((2*ii)-1))/2));
       sub_nu=[sub_nu sub_nu2];
       e_sub_nu2=e1(-1+floor((locs(2*ii)+locs((2*ii)-1))/2),i) ...
       -A1(-1+floor((locs(2*ii)+locs((2*ii)-1))/2));
       e_sub_nu=[e_sub_nu e_sub_nu2];
       else
       end
    end

    else
       for ii = 1:(length(locs)-1)/2;
       if locs(2*ii)-locs((2*ii)-1)<1.1*G(k) && ...
        locs(2*ii)-locs((2*ii)-1)>0.90*G(k)

       sub_nu2= nu1(-1+floor((locs(2*ii)+locs((2*ii)-1))/2));
       sub_nu=[sub_nu sub_nu2];
       e_sub_nu2=e1(-1+floor((locs(2*ii)+locs(2*ii-1))/2),i)...
       -A1(-1+floor((locs(2*ii)+locs((2*ii)-1))/2));
       e_sub_nu=[e_sub_nu e_sub_nu2];
        else
        end
       end
    end
end


%%%FP reconstruction%%%%

Ptot1=[sub_nu;e_sub_nu]';
```

```
Ptot=sortrows(Ptot1);
C=[];ia=[];ic=[];iv=[];
[C,ia,ic]=unique(Ptot(:,1));
iv=accumarray(ic,Ptot(:,2),[],@mean);


%%% Display Results %%%

fC=abs(fft(iv)).^2;
xC=((0:1:length(fC)-1)/(length(fC)-1))/(nu1((2))-nu1((1)));

d=abs(fft(A1)).^2;
xd=((0:1:length(d)-1)/(length(d)-1))/(nu1(2)-nu1(1));

fy=abs(fft(fabry1)).^2;
xfy=(0:1:length(fy)-1)/(length(fy)-1)/(nuf1(2)-nuf1(1));

fg=fft(strum);
xg=((0:1:length(fg)-1)/(length(fg)-1))/(nu1(2)-nu1(1));

dec=real(ifft((fft(A1)./fg')));
plot_dec=[dec(floor(length(dec)/2)+1:length(dec)); dec(1:floor(length(dec)/2))];
dec_f=abs(fft(dec)).^2;

figure(1);
subplot(1,2,1)
plot(C,iv);


end
end
```

References

1. Betzig, E., Trautman, J. K., Harris, T. D., Weiner, J. S. & Kostelak, R. L. Breaking the diffraction barrier: optical microscopy on a nanometric scale. *Science (New York, N.Y.)* **251,** 1468–70 (Mar. 1991).
2. Huang, F. M. & Zheludev, N. I. Super-Resolution without Evanescent Waves. *Nano Letters* **9,** 1249–1254 (Mar. 2009).
3. Igarashi, M. *et al.* New observations in neuroscience using superresolution microscopy. *The Journal of neuroscience : the official journal of the Society for Neuroscience* **38,** 9459–9467 (Oct. 2018).
4. Hell, S. W. & Wichmann, J. Breaking the diffraction resolution limit by stimulated emission: stimulated-emission-depletion fluorescence microscopy. *Optics Letters* **19,** 780 (June 1994).
5. Rust, M. J., Bates, M. & Zhuang, X. Sub-diffraction-limit imaging by stochastic optical reconstruction microscopy (STORM). *Nature Methods* **3,** 793–796 (Oct. 2006).
6. Betzig, E. *et al.* Imaging intracellular fluorescent proteins at nanometer resolution. *Science (New York, N.Y.)* **313,** 1642–5 (Sept. 2006).
7. Hess, S. T., Girirajan, T. P. & Mason, M. D. Ultra-High Resolution Imaging by Fluorescence Photoactivation Localization Microscopy. *Biophysical Journal* **91,** 4258–4272 (Dec. 2006).
8. Gazit, S., Szameit, A., Eldar, Y. C. & Segev, M. Super-resolution and reconstruction of sparse sub-wavelength images. *Optics Express* **17,** 23920 (Dec. 2009).
9. Candes, E. & Wakin, M. An Introduction To Compressive Sampling. *IEEE Signal Processing Magazine* **25,** 21–30 (Mar. 2008).
10. Zhu, L., Zhang, W., Elnatan, D. & Huang, B. Faster STORM using compressed sensing. *Nature Methods* **9,** 721–723 (July 2012).
11. Cheng, T., Chen, D., Yu, B. & Niu, H. Reconstruction of super-resolution STORM images using compressed sensing based on low-resolution raw images and interpolation. *Biomedical Optics Express* **8,** 2445 (May 2017).

12. Sidorenko, P. *et al. Super-resolution spectroscopy by compact representation* in *Frontiers in Optics 2012/Laser Science XXVIII* (OSA, Washington, D.C., Oct. 2012), FM3F.5.

13. Katz, O., Levitt, J. M. & Silberberg, Y. *Compressive Fourier Transform Spectroscopy* in *Frontiers in Optics 2010/Laser Science XXVI* (Optical Society of America, 2010), FTuE3.

14. Haykin, S. & Kesler, S. in *Nonlinear Methods of Spectral Analysis* 2nd ed. Chap. 2 (Springer-Verlag, New-York, 1983).

15. Kawata, S., Minami, K. & Minami, S. Superresolution of Fourier transform spectroscopy data by the maximum entropy method. *Applied Optics* **22,** 3593 (Nov. 1983).

16. Kauppinen, J. *et al. Fourier Transforms in Spectroscopy* tech. rep. (2001).

17. Mou-Yan, Z. & Unbehauen, R. A deconvolution method for spectroscopy. *Measurement Science and Technology* **6,** 482–487 (May 1995).

18. Lam, E. Y. & Goodman, J. W. Iterative statistical approach to blind image deconvolution. *J. Opt. Soc. Am. A* **17,** 1177–1184 (July 2000).

19. Pedrotti F. L., & Pedrotti, L.S. *Introduction to optics* (Prentice-Hall, Englewood Cliffs, N.J, 1987).

20. Blass, W. E. & Halsey, G. W. *Deconvolution of absorption spectra* 158 (Academic Press, New York, 1981).

Chapter 5

Experimental demonstration of super-resolved spectral reconstruction using a random laser

In this chapter we provide an experimental proof of concept for super-resolution spectroscopy using a frequency sparse sampling approach. We show that this can be done using a random laser as light source, taking advantage of its stochastic emission properties. In particular, by operating a random laser in its chaotic regime, its emission spectrum contains sharp random spikes that are sparsely distributed over its emission bandwidth and which are uncorrelated from shot to shot. These sparse collections of narrow spikes can be used to probe the spectral response of a sample and reconstruct a high-resolution response function using a 'bad', low resolution, spectrometer.

5.1 Description of the random laser sample

As described in Chapter 2, in a random laser there is no optical cavity in the traditional sense and the feedback mechanism needed for lasing is provided by multiple scattering. Due to the highly disordered arrangement of the disordered medium, laser emission from a random laser is typically characterized by very complex spectral features. Few technical points need to be considered in order to achieve super-resolved spectral measurements. First, the random laser source

should exhibit, on average, a suitable distribution of chaotic lasing modes with few sparse bright peaks, distributed over the emission spectrum. Secondly, the emission spectrum of each shot should be uncorrelated to the other shots. These requirements were fulfilled by adjusting the pump energy and the excitation volume. Overall the chaotic regime is easy to obtain and most random lasers operate here.

For this purpose, we realized a random laser sample made of a colloidal suspension of ZnO nanoparticles (10^{12} particles per cm^3, average particle diameter 200 nm) in a 5 mM solution of Rhodamine 6G in ethanol. The gain medium is optically pumped with a frequency-doubled pulsed Nd:YAG laser system (Ekspla, Mod. PL2143A), emitting pulses at 532 nm wavelength with a duration of 20 ps and repetition rate of 10 Hz. The chaotic lasing regime is obtained for a pumping condition just above threshold [1].

To optimize the efficiency of the spectral reconstruction method, it is important to consider the average number of modes that reach the lasing threshold (and hence generate a sharp peak) in each shot. According to the model developed by van der Molen *et al.* [2], the average number of lasing modes $\bar{N}$ can be written as:

$$\bar{N} = p \cdot N \tag{5.1}$$

where p is the probability of lasing and N the total number of modes in the system. By exploiting the usual balance between spontaneous and stimulated emission, and assuming that all modes contribute equally, this model predicts the β factor of a random laser to be $\beta = \bar{N}/N$, where β is equal to p. For picosecond excitation, p is in the range 0.05-0.1 [3]. The average number $\bar{N}$ of lasing modes in our sample is 5, while the total number of cavity modes can be estimated with the general relation $N = 8\pi n^3 V \Delta\lambda/\lambda^4$. For our sample this results in $N \sim 1800$ and p equal to 0.003, which is one order of magnitude lower than the typical value reported in literature.

In general, four main parameters that one can vary to get a different response from a random laser source are the i) optical gain, ii) scattering strength, iii) optical pumping power and iv) volume/shape of the pumping region. In turn, these parameters determine the two main features that we are interested in, namely the intrinsic width of random laser peaks (which ultimately poses a limit to the resolution achievable) and the average number of prominent peaks that are ob-

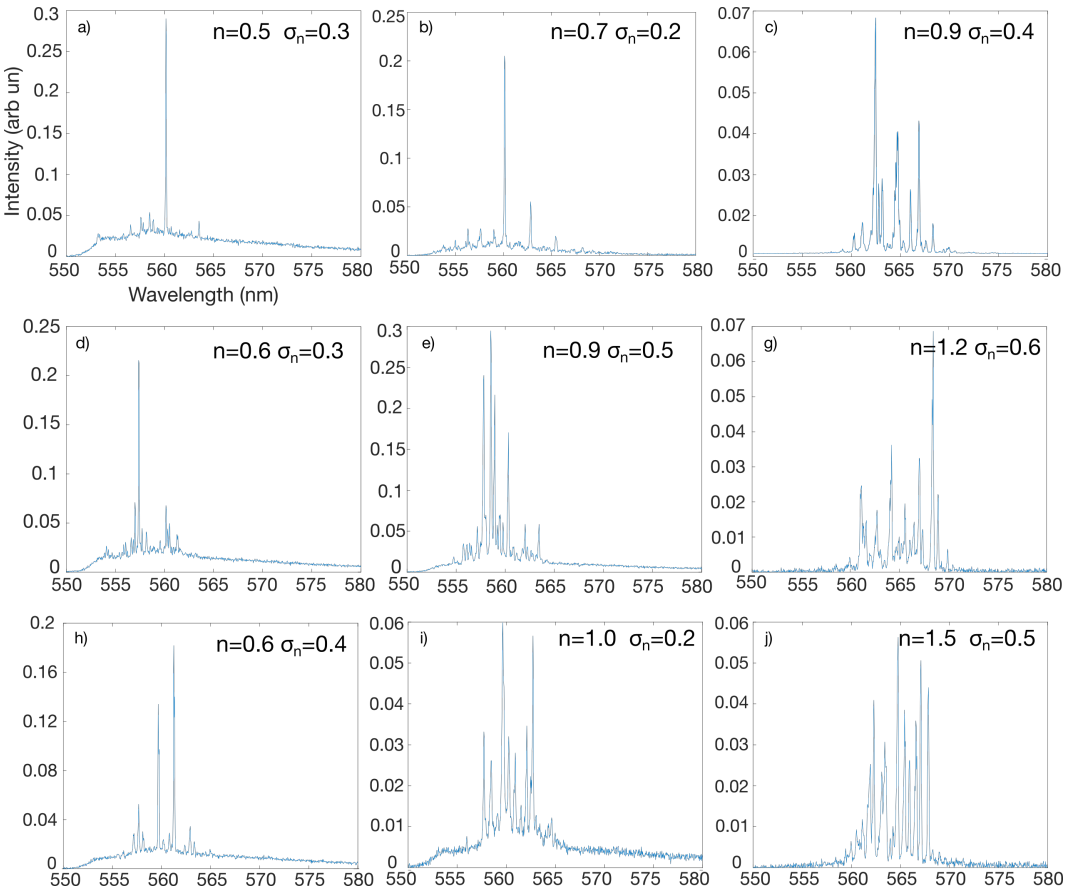

Figure 5.1: Single emission shots of nine mixtures of Rhodamine dissolved in ethanol containing scattering nanoparticles of ZnO. From left to right the dye concentration increases, from 5, 15, 45 mM, while from top to bottom the scatterer concentration varies from $1 \cdot 10^{12}$, $3 \cdot 10^{12}$, $6 \cdot 10^{12}$.

served in a single shot (which should not be too high to allow the correct identification of individual peaks, but also not too low so to collect a significant statistics more efficiently). Figure 5.1 shows an array of representative lasing shots from 9 different random laser mixtures where we have independently varied both the dye and ZnO nanoparticles concentrations while keeping all other conditions fixed. In detail, the panels are arranged with increasing dye concentration (5 mM, 15 mM, 45 mM) from left to right and increasing scatterer concentration (10^{12}, $3{\cdot}10^{12}$, $6{\cdot}10^{12}$ particles/cm^3) from top to bottom, showing the general trend observed when varying these parameters. These spectra are in agreement with previous reports in the literature, where it has been shown that starting from a particle concentration of about 10^{12} cm^{-3} the discrete spectral peaks appear before the collapse of the linewidth of the dye emission, indicating that the threshold for lasing with coherent feedback is lower than the threshold for lasing with incoherent feedback [4].

Given all the parameters that we can tune to adapt the spectral emission of our RL source, we have a large flexibility to tailor our random medium to suit our purpose. Successful spectral reconstruction can be performed using either the low gain (first column of Figure 5.1) and/or low scattering (first row) samples. In any case, suitable working conditions can be found even for samples with a higher density of lasing modes, as the average number of modes can be reduced to some extent by simply reducing the excitation spot and therefore the active medium volume. As long as one is working in a coherent feedback regime, these finer optimizations concur only marginally to the accuracy of the profile reconstruction and their main effect is that of slightly varying the number of spectra that one has to accumulate to attain a target signal-to-noise ratio. Even if the number of peaks for each mixture is subject to fluctuations, on average the emissions of samples in the first row (i.e., lowest nanoparticle concentration) contains fewer narrow peaks as compared to the other mixtures, as also expressed by the density of peaks per nanometer n, calculated as the average number of peaks in one spectrum divided by the FWHM of the gain curve. The optimal degree of spectral separation between lasing modes will depend on the properties of the spectrometer used, and in general should be set to be larger than its nominal resolution. In our case we varied the physical properties of the random laser used and its pumping conditions so to set an average number of 0.5 modes per nm, corresponding to an average separation of 2.5 times the instrumental resolution.

When the random laser is operated above threshold, well within the chaotic regime, the statistic of the intensity fluctuations follows the Lévy distribution [1, 5–7]. Figure 5.2.a shows the distribution of the peak frequencies for 300 emission shots. As expected, they follow approximatively the shape of the gain medium curve, with higher density around the frequency of maximum gain. Figure 5.2.b shows the histogram of the random laser peak intensities, exhibiting a power-law tail toward higher intensities. The histogram was fitted using a Stable probability density function (see Appendix A for further considerations about the Stable distribution and the working regimes of the random laser). From the fit an α value of 1.4 was extracted, indicating a distinct Lévy character for the distribution of peak intensities. Panel c) of Figure 5.2 shows three distinct histograms, respectively showing the distribution of peak intensities in three different spectral regions, around 527 THz, between 525 and 526 THz, and below 524 THz. In all these three cases the Lévy distribution character is clearly visible.

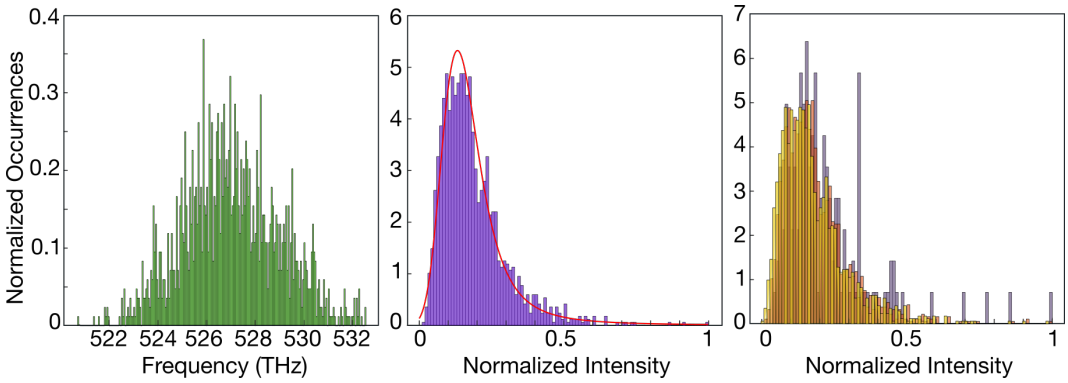

Figure 5.2: a) Distribution of the frequencies of the random laser peaks. b) Distribution of the peak intensities of the random laser, relative to the frequencies of panel a). The histogram data are fitted with a Stable probability density function and reveal the Lévy type regime. c) Distribution of the peak intensities of the random laser, relative to three different spectral regions: at 527 THz (yellow), 525-526 THz (orange) and in the tails, below 524 THz (grey).

5.2 Experimental set-up

In order to test our ideas in practice, we performed an experimental analysis using a custom-made Fabry-Perot etalon as an example. The etalon was realized

with a free spectral range of 0.3 THz and a maximum transmission contrast of 32% . A spectrometer was used with a resolution that did not allow to resolve the interference fringes of the etalon (FWHM = 2.8·FSR). The analysis was performed with a random laser and with a regular lamp for comparison. The outline of the experimental setup is sketched in Figure 5.3.a. The frequency doubled Nd:YAG laser was used to optically pump the random laser. The pump beam is collimated to a diameter of 8 mm to match the entrance pupil of a 10× microscope objective (NA 0.3, effective focal length 18 mm). The objective focuses the pump beam to a 10 µm spot size on the surface of the random laser sample. The same objective collects the random laser emission which is then divided into a reference beam and a probe beam using a beam splitter. The reference is directly focused by a lens (f = 50 mm) into one of the two entrances of a multimodal fiber bundle (fiber diameters 50 µm). The probe beam passes through the test sample and is then focused by a lens (f = 50 mm) at the other fiber entrance. The two fiber outputs (separated by 85 µm) are focused on the entrance slit of the monochromator and collected by a digital camera (Thorlabs, mod. DCC1240C, 1280×1024 pixel, 5.3 µm pixel size) synchronized with the pump pulse. The resolution of the spectrometer (Chromex, mod. 250is) can be tuned from an instrumental response of FWHM = 0.13 THz to 0.83 THz by changing the input slit aperture from 20 µm to completely open. In the latter case, the actual resolution is determined by the fiber output size and the entrance optics (3× magnification), resulting in an effective illuminated aperture of 150 µm at the focal plane of the monochromator. This FWHM corresponds to 2.8·FSR, and it is not sufficient to spectrally resolve the transmission function of the FP test sample. The latter configuration has been used to demonstrate our super-resolution method and reconstruct the transmission function of the test sample using the random laser source.

Figure 5.3.c shows the transmission function of the low finesse FP. The test sample has been fabricated using two uncoated IR flat mirrors. One side of each mirror has been coated with a few tens of nanometers of gold by sputtering deposition, resulting in a reflectivity of about 30%. The mirror inter-distance was set so to obtain the free spectral range of 0.3 THz, that corresponds to the narrowest FP modulation resolvable with the higher resolution configuration.

Figure 5.3.d reports the transmission spectrum of a single random laser shot as measured by the low-resolution spectrometer. The sample modulates the intensity of the probe signal with respect to the reference, but, as expected, the

visibility of the Fabry-Perot transfer function is completely lost even in the fluorescence background. Nonetheless, information on the transmission function of the sample is still contained in the relative heights of the peaks in the measured spectrum and can be retrieved by analyzing a large number of random laser shots. For that purpose, the center of each peak should be determined accurately, as well as the modulation of the peak height by the sample (obtained by comparing the transmission through the sample with the reference beam).

5.3 Analysis

The statistical analysis reported here is based on a set of single-shot random laser spectra acquired with the camera synchronized with the pump laser pulses. The selection of the peaks is based on the camera images, where a single resolution-limited random laser peak appears as a circle. Each circle is the image of the optical aperture at the focal plane of the spectrometer dispersed by the grating. When the apertures of the monochromator are fully open, the spectral resolution represented by the diameter of the circles is determined uniquely by the entrance optics. The observed diameter of 150 μm, corresponds to the spectral resolution of 0.83 THz. The spectral resolution was measured by replacing the random laser source with a passive scattering medium and illuminating it with a monochromatic pump beam.

The idea of our statistical analysis is shown in Figure 5.4. A set of 4000 single-shot random laser spectra is collected, each of them producing a double trace as shown. All traces contain both the transmitted signal (bottom) as well as the reference signal (top), so that the reference intensity profile is known for each individual random laser shot. Isolated random laser modes are selected on a single shot basis by an algorithm that identifies bright disks within a certain diameter range defined by the (low) spectral resolution of the spectrometer. Since the sampling has to be sparse, the average number of random modes above threshold should be small enough to have a vanishing probability of observing two peaks closer than the instrumental response function. For each disk selected in the bottom row (transmission signal), we determine its intensity by integrating over the area of the disk. This value is then normalized to the reference as found from the top row. Since random laser peaks have a finite linewidth, estimating the central

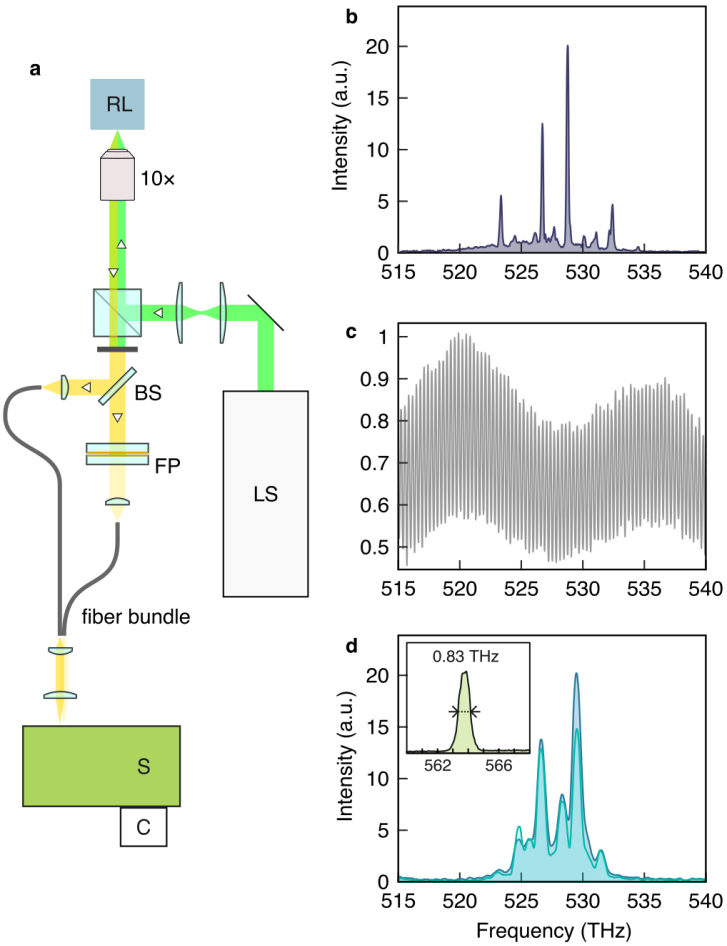

Figure 5.3: a) Scheme of the experimental setup. The random laser (RL) is optically excited by a pump laser (LS) which is focused using a 10× microscope objective. The same objective collimates the backscattered signal and the pump light is filtered out by an interference filter. A beam splitter (BS) divides the emission, a reference signal is focused to a multimodal fiber, while the probe passes through the sample (in this case a Fabry-Perot filter (FP)) before being focused into the second fiber. The two fiber cores are kept close so that they can be simultaneously focused at the entrance of the spectrometer (S) and their output collected by the same detector (C). b) Example of one of many (typically thousands) random emission spectra of the random laser source detected independently with higher spectral resolution. c) The transmission curve of the FP etalon sample that we are trying to characterize, as measured independently using a high-resolution spectrometer and a broad spectrum lamp. d) Example of a single shot transmission spectrum through the sample (cyan curve), using the random laser as a light source and the experimental scheme of the panel (a) with a low-resolution spectrometer. The center frequency of each peak is determined accurately, as well as the value of the transmission compared to the reference measurement (light blue curve) at that specific frequency.

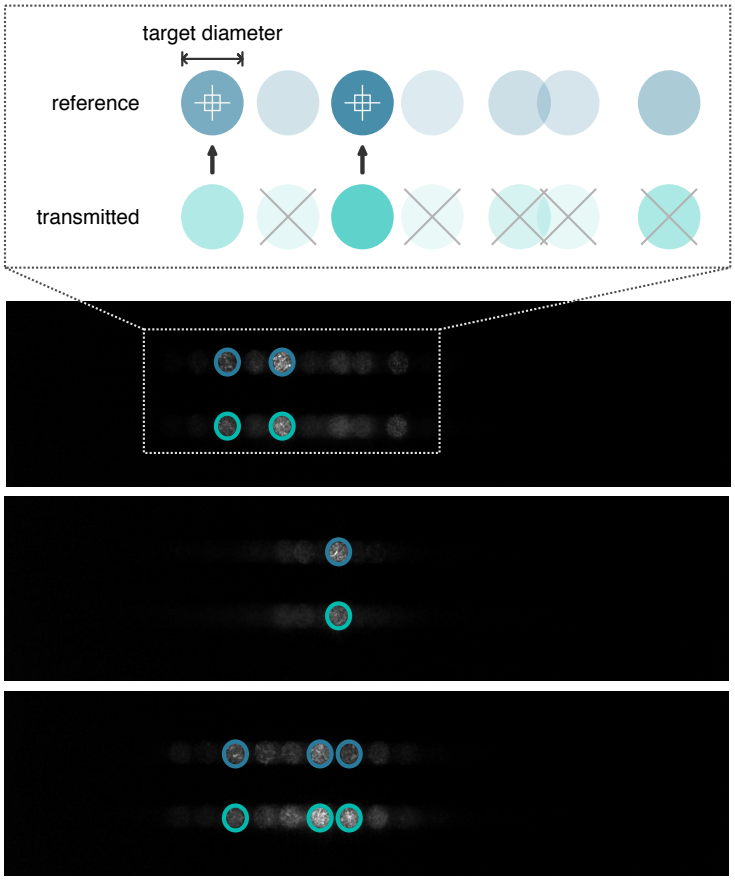

Figure 5.4: Low-resolution peak selection. Exemplary low-resolution spectra measured by the CMOS camera under random laser illumination. The top and bottom rows in each frame correspond to the reference and transmitted signal, respectively. An algorithm finds the most intense, non-overlapping circles within a fixed diameter range. Each shot allows to reconstruct a few points of the target function.

frequency of each lasing mode requires some extra care as the transmitted disks might appear at a slightly detuned frequency due to possibly asymmetric modulation through the unknown transfer function. In our experimental case, using an average peak width of 0.19 THz, the resulting order of magnitude of the expected apparent deviations lead to a negligible correction. However, our algorithm is inherently robust against even stronger deviations as long as the spectral sparsity condition is fulfilled. In fact, we use the center position of each peak using the disk centers of the reference signal – and not the probe signal – which did not interact with the spectral filter and therefore shows each peak centered at its original frequency. The procedure of sparse sampling in the frequency domain allows to reconstruct the transmission function of the sample. The final result is shown in Figure 5.5.a. One can clearly see that the transmission function of the Fabry-Perot etalon is reconstructed with all its relevant features present. The unrefined fabrication procedure of the FP allowed us to obtain a rich spectral benchmark sample exhibiting both rapidly-varying and slowly-varying spectral features and the reconstruction procedure successfully retrieves all these features, including both the FP spectrum and its slant underlying background.

For comparison, when the transmission spectrum is measured using a standard lamp as light source, the etalon transmission function cannot be retrieved even when averaging over the same amount of spectra to reduce measurement noise (See Figure 5.5.b.). The effectiveness of the method is further highlighted by analyzing the results in the Fourier domain. The periodicity of the transmission function of the Fabry-Perot etalon is clearly retrieved when using the random laser, while it is lost in the measurements with the lamp (See Figs. 5.5.c-d).

According to the numerical results reported on Figure 4.4 in Chapter 4, the signal-to-noise ratio of the recovered transmission function grows by increasing the number of spectra. However this is always the case under white noise conditions, and, experimentally, we avoid collecting data for a longer period than ~ 400 s in order to exclude possible variations in the density of the scattering particles in the sample, due to the aggregation and precipitation processes. In general, if one wants to set a higher reconstruction fidelity, care must be taken that the overall measurement duration does not exceed the stability time-scale of the spectral filter itself due to e.g., ambient temperature drifts. Alternatively, one can simply use a pump laser with a higher repetition rate (e.g., a typical frequency-doubled Nd:YAG laser with a 10 kHz repetition rate), by which one can easily

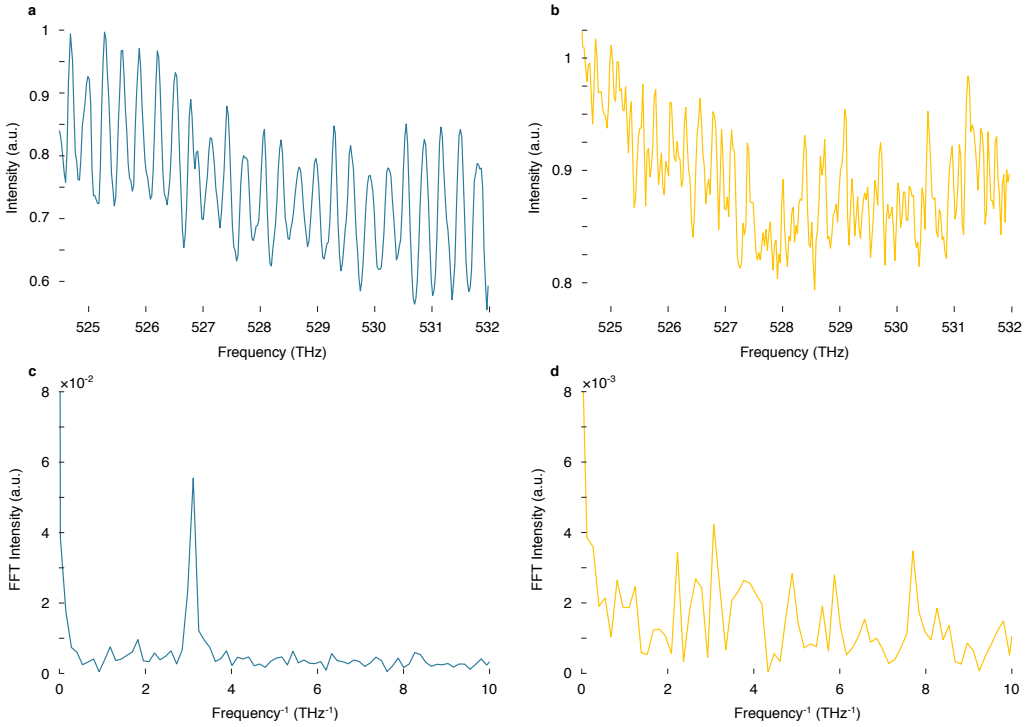

Figure 5.5: a) Transmission curve as obtained by sparse sampling using the random laser. The target transmission function is well reproduced. b) Transmission curve as obtained with a common lamp for comparison. As expected the transmission function of the Fabry-Perot etalon is lost due to convolution with the instrumental response function. Deconvolution is not successful in retrieving the original contrast since the target signal is lost in the noise. c) Fourier transform of (a). The peak corresponds to the inverse of the free spectral range of the etalon, confirming that the target function is well reproduced. d) Fourier transform of the transmission curve measured with the common lamp.

reduce the measurement time required to collect the same number of spectra below a sub-second time scale.

5.3.1 Validity limits and fundamental bounds

A key issue that deserves to be discussed in details is the resolution enhancement obtainable with the present technique. In the following we try to explain the different experimental aspects that contribute to define the resolution. The ultimate resolution limit is represented by the finite linewidth of the single random laser peaks, which should be finer than the features that one wants to resolve. If this is not the case, the stochastic reconstruction can still be performed but the final spectrum will be characterized by a reduced contrast of its sharpest features. Indeed, if the linewidth of the random laser was broad, for example as large as few FP filter resonances, the reconstructed transmission curve would be the affected by the convolution of the lasing peak with the filter transfer function. Since the spectrometer resolution used for the characterizations (0.13 THz) was slightly better than the measured linewidth, we can conservatively assume that the measured value is an upper limit to the true line width of the modes. In any case, this number is a typical value for random lasers based on liquid dye solutions, even though it is possible to engineer the RL or the pumping strategy to obtain much narrower linewidths (see, e.g [8]) which can directly improve the resolution limit of the reconstruction technique. The second important factor, in analogy with the stochastic super-resolution microscopy techniques, is represented by the (spectral) sparsity which is necessary to correctly identify the laser peaks and therefore their center frequency. These are the two mandatory requirements, i.e., narrowness and sparsity of the peaks, for the technique to work. If they are not both satisfied the transfer function can still be retrieved but a deconvolution process needs to be applied to finally recover the original contrast. Another factor, which is more of a practical limit than an actual requirement, is represented by the number of pixels of the camera which samples the spectral response (point spread function) of the spectrometer. In close connection to the microscopy case, to achieve a sub-pixel centroid estimation, it is necessary that each peak be sampled with a minimum number of points. This final condition is easily attainable with the vast majority of consumer CMOS camera as that used in our experiment. Considering all these aspects, we have demonstrated a spec-

tral resolution enhancement factor of ~3. This enhancement does not have an upper limit in principle as the initial resolution of the spectrometer that one is using can be arbitrarily coarse as long as the sparsity requirement is satisfied.

5.3.2 The roles of sparsity and randomness

The concept of "sparsity" can be related to different fields and concepts and its specific meaning should be further clarified. For the purpose of this proof-of-concept, our algorithm relies exclusively on the accumulation of a sufficiently large statistical ensemble. In this respect, we refer to the concept of sparsity only in relation to the inherent spectral separation that is typically observed between RL peaks. Nonetheless, it could be appropriate to further refine the application of our technique using e.g., compressed sensing, as demonstrated by recent applications to conventional stochastic microscopy techniques [9]. As in the case of STORM microscopy, however, resorting to compressed sensing would not represent an enabling factor for the technique but rather just a convenient way to reduce the acquisition time. More in detail, one could follow e.g., the approach described in [9] to be able to use random lasers exhibiting, on average, a higher number of discrete peaks in each laser shot. However, as discussed before, a much more straightforward way to reduce acquisition time would be just that of increasing the pumping repetition rate of the random laser. As far as randomness is concerned, it is not an inherent requirement for this technique to work. Indeed, a single narrow frequency line from an ideal tunable laser could be swept over the frequency range of interest to reconstruct a given transmission function with a higher resolution than that offered by the spectrometer. The emphasis on the chaotic lasing regime is due to the fact that this ensures both narrow line widths and a uniform sampling over the emission band.

5.4 Comparison with state of the art techniques

The method we described allows to resolve, in the frequency domain, spectral features below the instrumental response function of a spectrometer similarly to how stochastic super-resolution microscopy methods allow to resolve fine spatial features below the diffraction limit. In this respect, our method offers similar

pros and cons as those characterizing these imaging methods. As previously discussed, a well-established approach to improve the resolution of spectroscopic data is represented by deconvolution [10]. Deconvolution encompasses a family of data processing methods that require or assume the knowledge of the instrumental response function and try to correct for it. When this is possible, deconvolution has been shown to enhance the resolution of spectral data and is therefore considered as a standard tool [11]. Among all available deconvolution methods, the constrained deconvolution algorithm proposed by Jansson and other methods such as the maximum likelihood, the maximum entropy and the alternating projection methods are also known for their utility [12, 13], yet all these methods require a priori knowledge of the instrumental response function (also referred to as blur function or broadening function). In practice, however, the exact shape of the response function cannot be known and it is typically assumed to be Gaussian. More recently, blind deconvolution has been proposed to alleviate this problem, being a deconvolution procedure where one tries to iteratively refine an initial guess on the assumed instrumental response function according to certain constraints. Even so, it is worth stressing that discrete deconvolution, in any of its forms, belongs to the mathematical class of ill-conditioned inverse problems, meaning that its output is not stable against small perturbations such as those typically provided by acquisition noise. Regularization approaches can be applied in some circumstances [14], but in general, in any deconvolution approach, one is obliged to search only for solutions that are compatible with some a priori expectation on the experimental data, and satisfy additional constraints provided by prior information coming from the physical problem that is being investigated.

In our experimental measurements we have demonstrated a spectral enhancement factor of about 3, which is the same limit that can be achieved with state-of-the-art deconvolution-based approaches in low-noise conditions. However, in contrast to deconvolution, our approach does not have any upper limit on the resolution enhancement that can be achieved. Furthermore, our approach does not require prior knowledge or an exact characterization of the instrumental response function, as it only relies on the position of the geometric center of the observed disk-shaped region, or of any other kind of spectral response that one can have. This makes our method particularly robust against possible acquisition noise. As remarked in Section 5.3.2, compressive sensing methods should be

straightforwardly applicable to the reconstruction technique in order to reduce the number of spectra required to obtain a certain signal-to-noise level. In compressive ghost imaging, for example, the reconstruction algorithms search for the sparsest image in the compressive basis which fulfills the requirement that the number of measured random projections was slightly greater or equal than the number of the image grid points, in contrast to conventional ghost imaging where the requirement is much greater. The choice of randomness is due to the fact that with more likely these image projection were linearly independent [15].

An alternative high-resolution spectroscopy technique that should also be mentioned is that based on the use of frequency combs, which in a sense resembles our own approach since it exploits a discrete (i.e., spectrally sparse) excitation spectrum to probe an unknown transfer function. Initially invented for frequency metrology, frequency combs are also enabling novel approaches to spectroscopy over broad spectral bandwidths that are of particular relevance to molecules [16]. In the simplest spectroscopy experiment a frequency comb can be used as a broadband light source which interrogates an absorbing sample. In fact, most of the times a spectrometer is not capable of resolving individual comb lines, unless one uses frequency combs generated by a micro-resonator or filtered through a Fabry-Perot cavity to increase the comb line spacing to exceed the spectrograph resolution [17]. By doing so, high resolution gas-phase absorption spectra can be obtained by tuning the comb line inside one free spectral range. On the other hand, of course the combination of a frequency comb and an external cavity poses high costs and strict stability requirements. Conversely, our proof of concept takes advantage of an intrinsic property of a random lasing light source, which can conveniently generate a stochastic peaks distributed over the gain medium curve. This approach does not require any particular spectral stability of the source, cavity alignment nor tuning.

We should note that at this stage, even if the light source used for the experiment is an optically pumped random laser, which is very cheap and easy to realize, it still needs a pump laser to work. Since laser sources are already used pervasively in most spectroscopic techniques, at the moment our spectroscopy technique should be comparable in terms of power consumption to other conventional spectroscopic techniques. However, among the existing realizations of random lasers, electrically pumped RLs are appealing candidates in terms of their high efficiency and low power requirements. Several realizations of electri-

cally pumped random lasers (EPRL) have been reported in the literature, which might represent a competitive alternative. As an outlook perspective to this thesis work, we are actually planning to explore this possibility using an EPRL in the THz range, which is indeed of interest given the very low footprint with respect to typical sources/detectors in this frequency range.

Appendices

A Random laser threshold and stable distributions

Among the various intriguing properties of random lasers, one that remains fundamentally relevant to all studies is the random lasing threshold. When the pump excitation reaches a critical value, the random laser system crosses the threshold and the emission characteristics change. While in conventional lasers the emission intensity diverges (with a certain level of approximation) at threshold excitation, in the case of random lasers different indicators are used to identify the threshold, depending on their composition. When using broadband dyes, strong fluctuations in both intensity and bandwidth are a commonly observed behavior [18, 19].

The intensity fluctuations, depending upon parameters such as the pump energy, the system size and disorder strength, an interesting consequence of these strong fluctuations is that the intensity distribution does not obey regular gaussian statistics, but rather becomes of the Lévy type. Lévy distributions have an infinite variance, owing to the occurrence of rare but very large values, and are characterized by a slowly decaying tail (power-law trend).

Since the emission intensities involve mixed statistical features, we make use of α-stable distributions to model the heavy-tailed distributions observed in the lasing mode intensities, as also done by Uppu & Mujumdar [7].

Stable distributions are a class of probability distributions suitable for modeling heavy tails and skewness. The stable distribution results from an application of the Generalized Central Limit Theorem, which states that the limit of normalized sums of independent identically distributed variables is stable [20]. Several different parameterizations exist for the stable distribution. We use the parameterization described in [21] (2).

$$\begin{cases} \exp\Big\{\big(-\gamma^{\alpha}|t|^{\alpha}\big[1+i\beta\,\mathrm{sign}(t)\tan\frac{\pi\alpha}{2}\left((\gamma|t|)^{1-\alpha}-1\right)\big]+i\delta t\big)\Big\} & \text{for } \alpha = 1 \\ \exp\Big\{\big(-\gamma|t|\big[1+i\beta\,\mathrm{sign}(t)\,\frac{2}{\pi}\ln\big(\gamma|t|\big)\big]+i\delta t\big)\Big\} & \text{for } \alpha \neq 1 \end{cases} \tag{2}$$

Most members of the stable distribution family do not have an explicit probability density function. The stable distribution has three special cases: the Nor-

mal distribution, the Cauchy distribution, and the Lévy distribution. These distributions are notable because they have closed-form probability density functions. The first shape parameter, α, describes the tails of the distribution, and ranges from 0 to 2. The second shape parameter, β, describes the skewness of the distribution ($-1 \leq \beta \leq 1$). If $\beta = 0$, then the distribution is symmetric. If $\beta > 0$, then the distribution is right-skewed and if $\beta < 0$, then the distribution is left-skewed. The third parameter δ represents the location parameter ($-\infty \leq \delta \leq \infty$). When the parameter α is equal to 2 it indicates a Gaussian behavior, and the value of β has no effect, then the normal distribution is usually associated with $\beta = 0$. The Lévy distribution is a special case of the stable distribution where $\alpha = 0.5$ and $\beta = 1$.

In many works the α parameter has been used to identify the different working regimes of the random laser [1, 7]: below threshold a Gaussian regime is observed, followed, at threshold, by an abrupt transition into a Lévy regime. Well above the threshold, a gradual crossover toward a second Gaussian regime occurs. The Levy regime is weak ($\alpha \lesssim 2$) or strong ($\alpha \lesssim 1$) also depending on the system size, for example, for larger excitation volume, at threshold conditions, the levy statistic is less prominent. In this configuration many lasing modes have reached the threshold, and all of them compete for gain. Then, a situation where two or even a single mode which deplete the gain is improbable, however it is exactly this kind of fluctuations that is responsible for the tail of the Lévy distribution, or, in other words, results in an α parameter below unity.

B MATLAB code for peak selection

```
clear all;close all
nf1=274;
%gb=[];
gb=[0 1 2 3 4 5 6 7 8 9 10 11 12 13 14 15];
XU=[];
YU=[];
YD=[];
x=[1:1280];

a=imread('rl3_fp_670nm_g600_200um_0.tif',2);
bck=imread('bck_g600_1.tif',1);
[~,idx]=findpeaks(smooth(mean(a(:,:,2),2),30)/max(smooth(mean(a(:,:,2),2),30)), ...
'MinPeakHeight',0.2,'MinPeakProminence',0.2);
       cut1u=idx(2)-30;
       cut2u=idx(2)+30;

       cut1d=idx(1)-30;
       cut2d=idx(1)+30;
R=15;

for k=gb

    for i=1:nf1
       str=['b0=imread(''rl3_fp_670nm_g600_200um_' num2str(k) '.tif'',' ...
       num2str(i) ');'];eval(str);

        b0u=b0(cut1u:cut2u,:,2)-bck(cut1u:cut2u,:,2);
        b0d=b0(cut1d:cut2d,:,2)-bck(cut1u:cut2u,:,2);

       v=double(max(max(b0u)));
       vv=v/255;
       J=imadjust(b0u,[0 vv],[0 1],1);
        [centers, radii, metric] = imfindcircles(J,[14 25],'Sensitivity',0.94);

        xu=[];
       if not(isempty(centers))
               xu= centers(:,1);
               XU=[XU; xu];
```

```
            for ii=1:length(centers(:,1))
                mn=[];
                yu=[];
                yd=[];
               for l=1:1280
                     for s=1:(cut2u-cut1u)
                         if ((l-round(centers(ii,1)))^2+ ...
                         (s-round(centers(ii,2)))^2)<R^2
                         yu0=b0u(s,l);
                         yd0=b0d(s,l);
                         yu=[yu yu0];
                         yd=[yd yd0];
                         mn0=[l s];
                         mn=[mn; mn0];
                         end
                     end
                end
               YU0=mean(yu);
               YD0=mean(yd);
               YU=[YU YU0];
               YD=[YD YD0];
            end
        end
    end
  k
end

Ptot1=[XU (YD./YU)'];
Ptot=sortrows(Ptot1);

[C,~,ic]=unique(Ptot(:,1));
iv=accumarray(ic,Ptot(:,2),[],@mean);

xx=[390:1:900];
yy=[];
My=[];
my=[];
for ii=1:length(xx)-1;
    idx=find(C<xx(ii+1) & C>=xx(ii));
    idy=mean(iv(idx));
    yy=[yy idy];
    My=[My max(iv(idx))];
```

```
    my=[my min(iv(idx))];
end
   figure;plot(xx(2:end),yy,); xlim([415 738]);


  for jj=1:length(yy)
      if  isnan(yy(jj));
          yy(jj)=0;
      end
  end


   F=abs(fft(yy));
   FX=((0:1:length(F)-1)/(length(F)-1))/(xx(2)-xx(1));
   figure(4);plot(FX,F/max(F));
```

References

1. Uppu, R., Tiwari, A. K. & Mujumdar, S. Identification of statistical regimes and crossovers in coherent random laser emission. *Optics Letters* **37,** 662 (Feb. 2012).
2. Van der Molen, K. L., Mosk, A. P. & Lagendijk, A. Intrinsic intensity fluctuations in random lasers. *Physical Review A* **74,** 053808 (Nov. 2006).
3. Van Soest, G. & Lagendijk, A. β factor in a random laser. *Physical Review E* **65,** 047601 (Mar. 2002).
4. Cao, H., Xu, J. Y., Chang, S.-H. & Ho, S. T. Transition from amplified spontaneous emission to laser action in strongly scattering media. *Phys. Rev. E* **61,** 1985 (2000).
5. Araújo, C., Gomes, A. & Raposo, E. Lévy Statistics and the Glassy Behavior of Light in Random Fiber Lasers. *Applied Sciences* **7,** 644 (June 2017).
6. Sharma, D., Ramachandran, H. & Kumar, N. Lévy statistics of emission from a novel random amplifying medium: an optical realization of the Arrhenius cascade. *Optics Letters* **31,** 1806 (June 2006).
7. Uppu, R. & Mujumdar, S. Lévy exponents as universal identifiers of threshold and criticality in random lasers. *Phys. Rev. A* **90,** 025801 (2 2014).
8. Bachelard, N., Gigan, S., Noblin, X. & Sebbah, P. Adaptive pumping for spectral control of random lasers. *Nature Physics* **10,** 426–431 (2014).
9. Zhu, L., Zhang, W., Elnatan, D. & Huang, B. Faster STORM using compressed sensing. *Nature Methods* **9,** 721–723 (July 2012).
10. Mou-Yan, Z. & Unbehauen, R. A deconvolution method for spectroscopy. *Measurement Science and Technology* **6,** 482–487 (May 1995).
11. Blass, W. E. & Halsey, G. W. *Deconvolution of absorption spectra* 158 (Academic Press, New York, 1981).
12. Jansson, P. A. *Deconvolution : with applications in spectroscopy* 342 (Academic Press, New York, 1984).
13. Frieden, B. R. *Probability, Statistical Optics, and Data Testing : a Problem Solving Approach* (Springer Berlin Heidelberg, 1983).

14. Iqbal, M. Deconvolution and regularization for numerical solutions of incorrectly posed problems. *Journal of Computational and Applied Mathematics* **151,** 463–476 (Feb. 2003).

15. Katz, O., Bromberg, Y. & Silberberg, Y. Compressive ghost imaging. *Applied Physics Letters* **95,** 131110 (Sept. 2009).

16. Picqué, N. & Hänsch, T. W. Frequency comb spectroscopy. *Nature Photonics* **13,** 146–157 (2019).

17. Gohle, C., Stein, B., Schliesser, A., Udem, T. & Hänsch, T. W. Frequency Comb Vernier Spectroscopy for Broadband, High-Resolution, High-Sensitivity Absorption and Dispersion Spectra. *Phys. Rev. Lett.* **99,** 263902 (2007).

18. Mujumdar, S., Ricci, M., Torre, R. & Wiersma, D. S. Amplified extended modes in random lasers. *Physical Review Letters* **93** (2004).

19. Mujumdar, S., Türck, V., Torre, R. & Wiersma, D. S. Chaotic behavior of a random laser with static disorder. *Phys. Rev. A* **76,** 033807 (Sept. 2007).

20. S., Š. *Stable Distributions and Random Walks. In: Probability for Physicists. Graduate Texts in Physics* (Springer, Cam, 2016).

21. Nolan, J. Stable Distribution: Models for Heavy-Tailed data (Jan. 2014).

Acknowledgments

The work of this three years Phd course is the result of the help and the advice of many persons, that I really feel to thank. First of all, my advisor, Diederik, to give me the opportunity to work on these interesting subjects. Diederik gave me the motivation and a large amount of autonomy, which allowed my to try different research approaches, but at the same time a lot of support on how to conduct practically my experiments.
I want warmly to thank Renato who gave me precious advices, brilliant discussions concerning my experiments and help in many difficult moments. Thanks for the time you dedicated to me.
Thanks to my friends and colleagues of the Complex Systems group, Sara, Flavia, Daniele, Camilla, Lorenzo, Francesco e Giacomo, for to their pleasantness and competence, the stimulating group meetings each Thursday, but also the delirious discussions and the laugher about physics and much more in our breaks. Thanks again to Lorenzo, for your decisive help and for all the myriad of extraordinary enlightenment s you gave to me. Without your efforts and brilliant presence this work would not have been what it is, and thanks also for your big smiles and constant support.
The last, stronger thank goes to the friends, colleagues, the best experimental physicists of my heart, Paolo e Andrea, which makes this PhD course the most interesting, funny, mad and unforgettable that a student could immagine. Thank you for your constant presence and patience, for these three years the Lab. 20 has been my family! And as in all the respectable families joys and pains are shared. Thanks for the constant help you gave me in the realization of the experiments and for all the stuff you have taught to me.
And finally, what to say Sara, thank you?... Every word is useless, I think I am very lucky to have found a friend like you.